Electronic Supplementary Information

for

Aluminium complexes containing salicylbenzothiazole ligands and their application in the ring-opening polymerisation of *rac*-lactide and ε-caprolactone

Chutikan Nakonkhet,[a] *Tanin Nanok,*[b] *Worawat Wattanathana*[c] *Pitak Chuawong*[d] *and Pimpa Hormnirun*[*,a]

[a]Laboratory of Catalysts and Advanced Polymer Materials, Department of Chemistry and Center of Excellence for Innovation in Chemistry, Faculty of Science, Kasetsart University, Bangkok 10900, Thailand

[b]Department of Chemistry, Faculty of Science, Kasetsart University, Bangkok 10900, Thailand

[c]Department of Materials Engineering, Faculty of Engineering, Kasetsart University, Bangkok 10900, Thailand.

[d]Department of Chemistry and Center of Excellence for Innovation in Chemistry, Faculty of Science, and Special Research Unit for Advanced Magnetic Resonance (AMR), Kasetsart University, Bangkok 10900, Thailand

*E-mail: fscipph@ku.ac.th

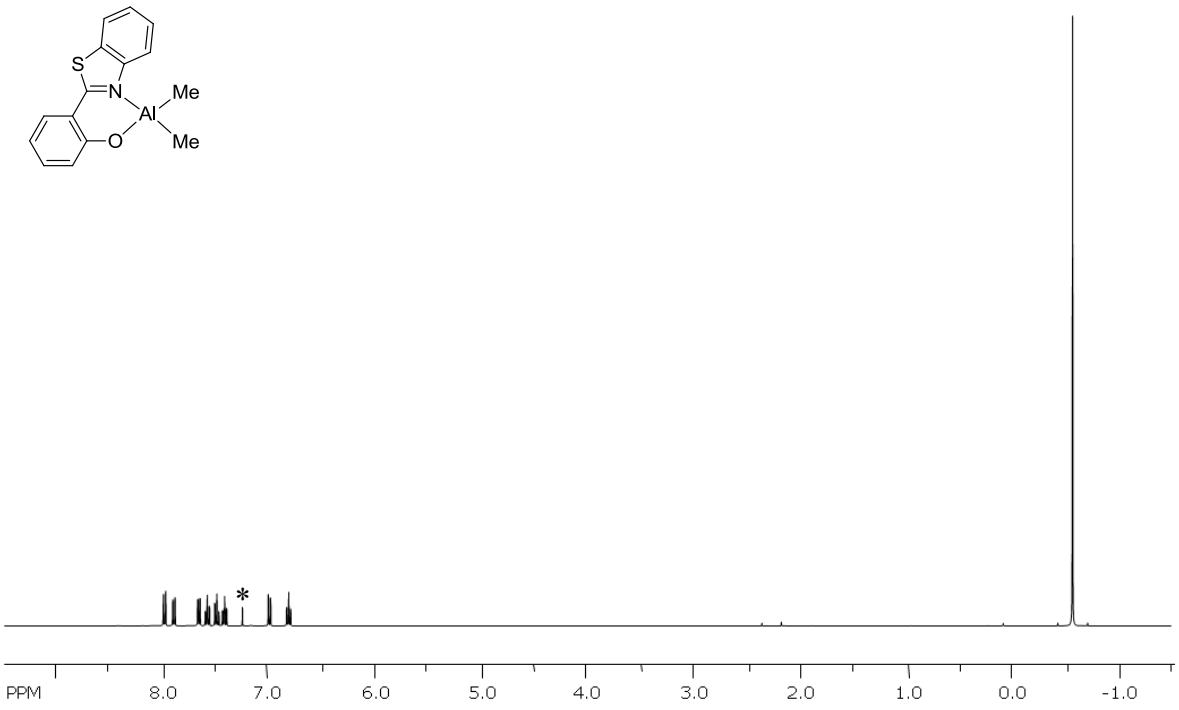

Fig. S1. ^{1}H NMR spectrum of **1a** in $CDCl_3$ at 298 K (* = solvent residue signal).

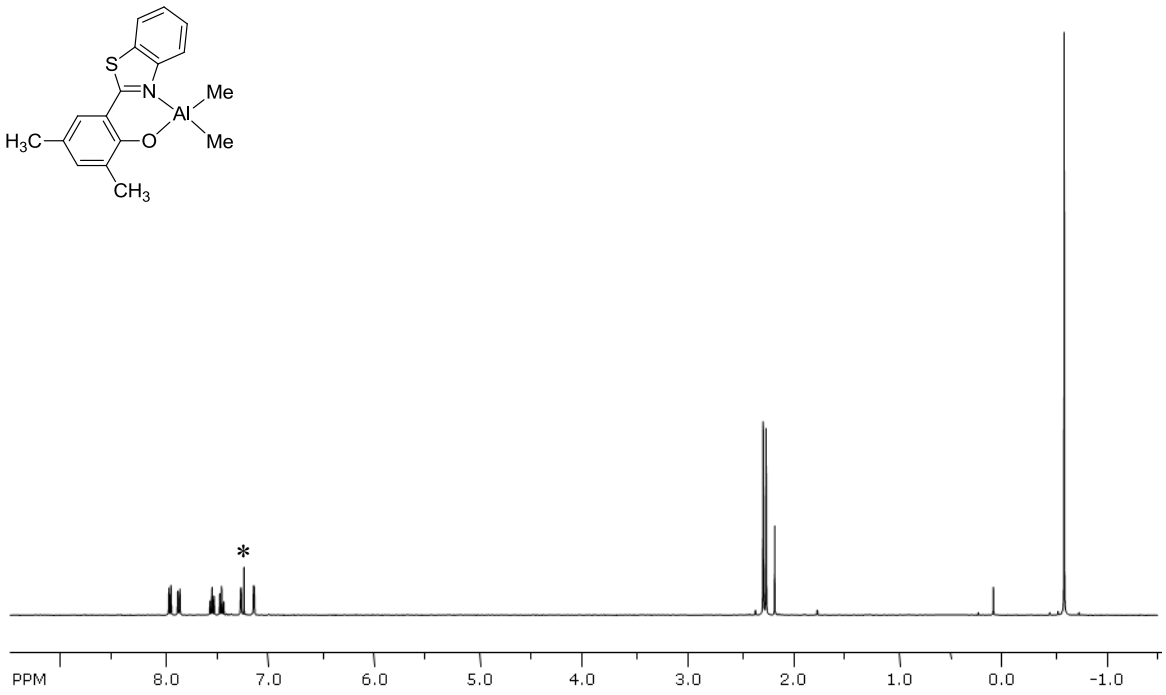

Fig. S2 ^{1}H NMR spectrum of **2a** in $CDCl_3$ at 298 K (* = solvent residue signal).

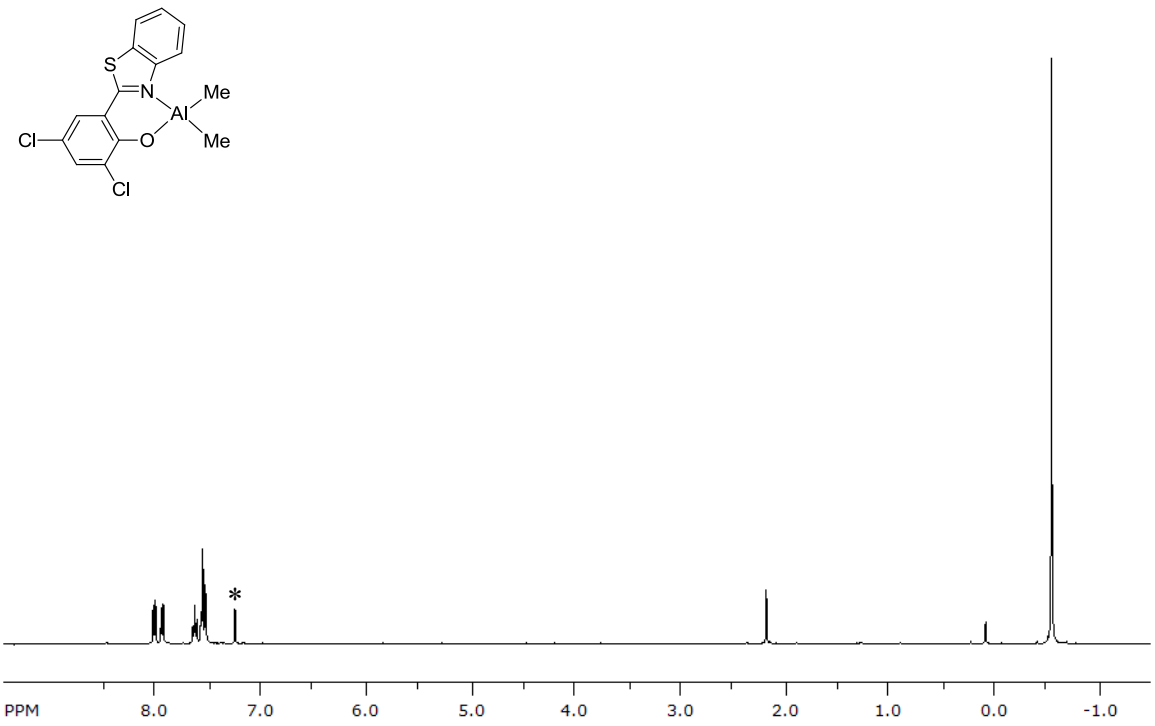

Fig. S3 ^{1}H NMR spectrum of **3a** in $CDCl_3$ at 298 K (* = solvent residue signal).

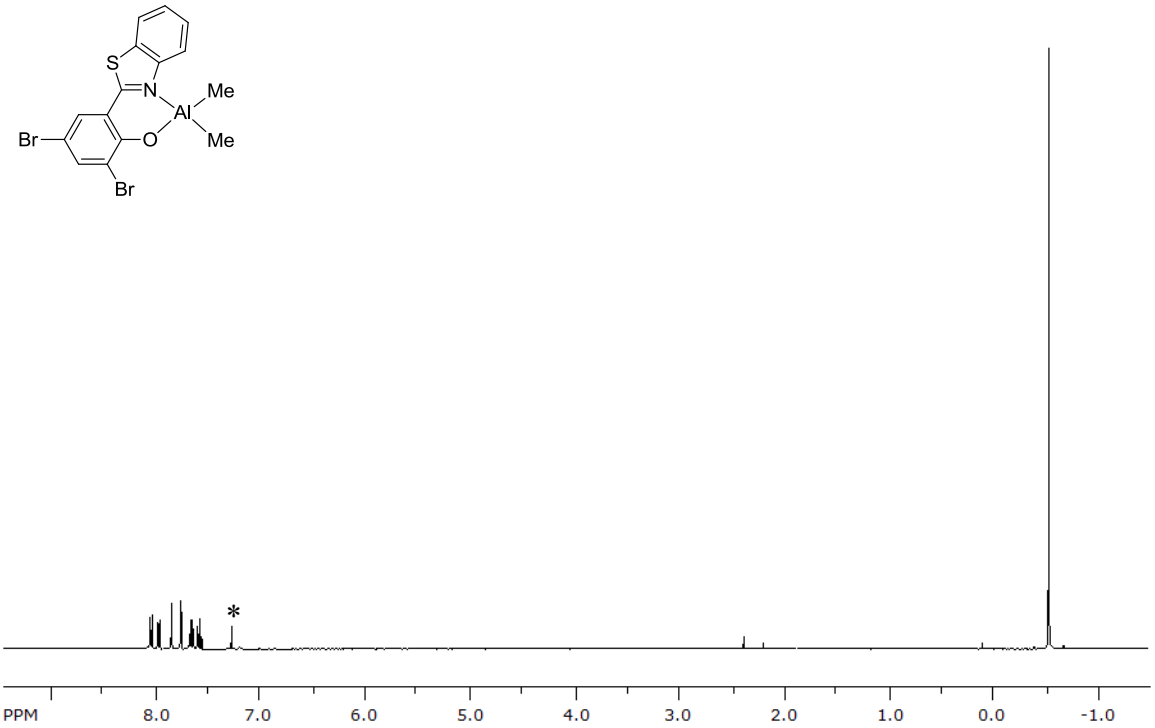

Fig. S4 ^{1}H NMR spectrum of **4a** in $CDCl_3$ at 298 K (* = solvent residue signal).

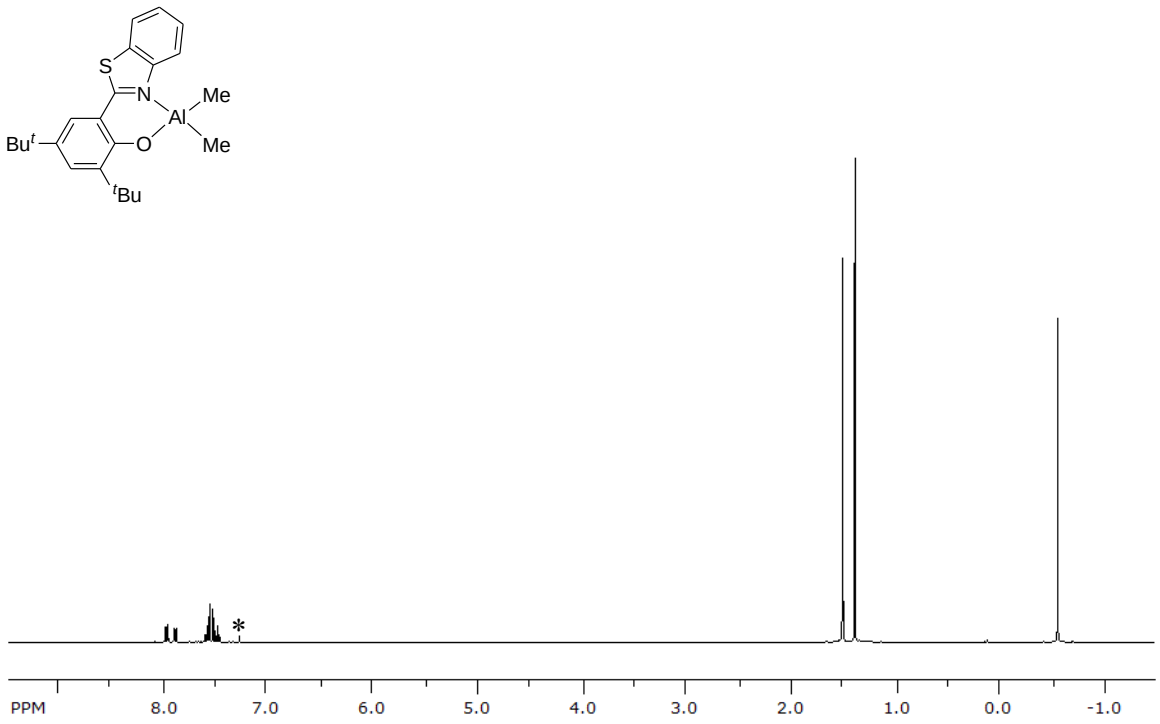

Fig. S5 ^{1}H NMR spectrum of **5a** in $CDCl_3$ at 298 K (* = solvent residue signal).

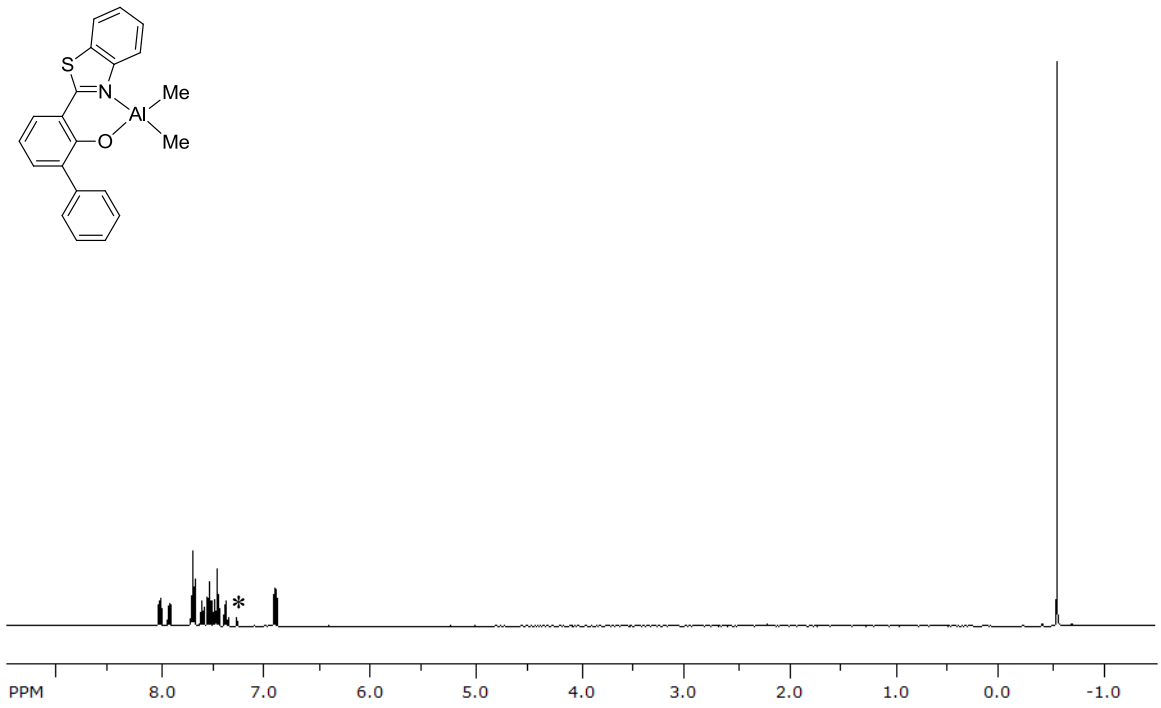

Fig. S6 ^{1}H NMR spectrum of **6a** in $CDCl_3$ at 298 K (* = solvent residue signal).

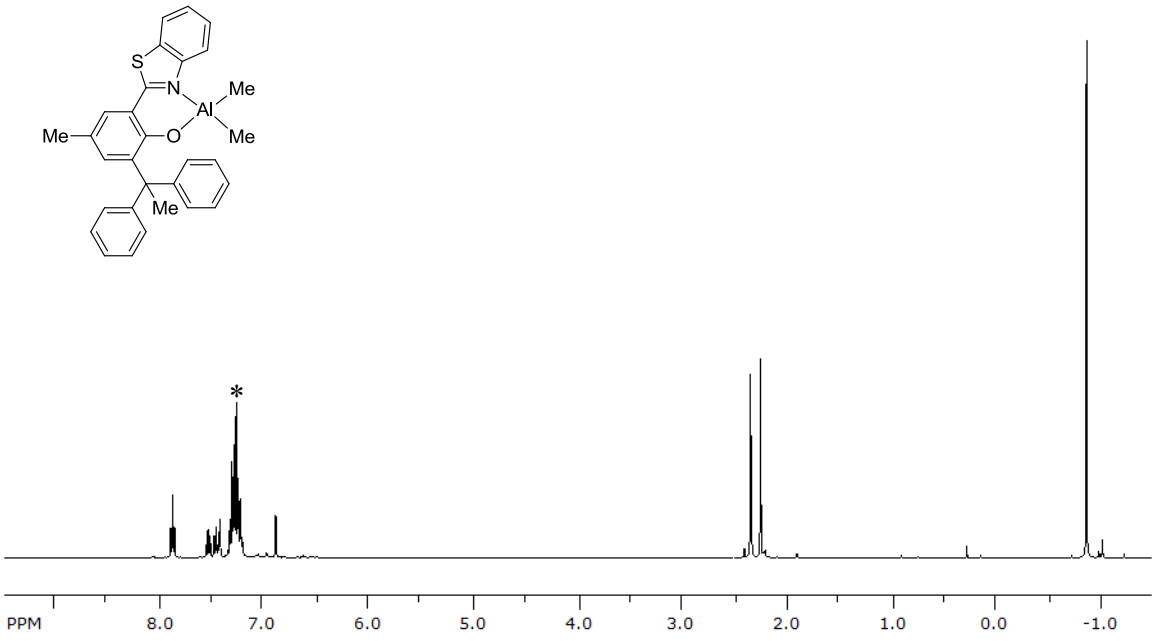

Fig. S7 ^{1}H NMR spectrum of **7a** in $CDCl_3$ at 298 K

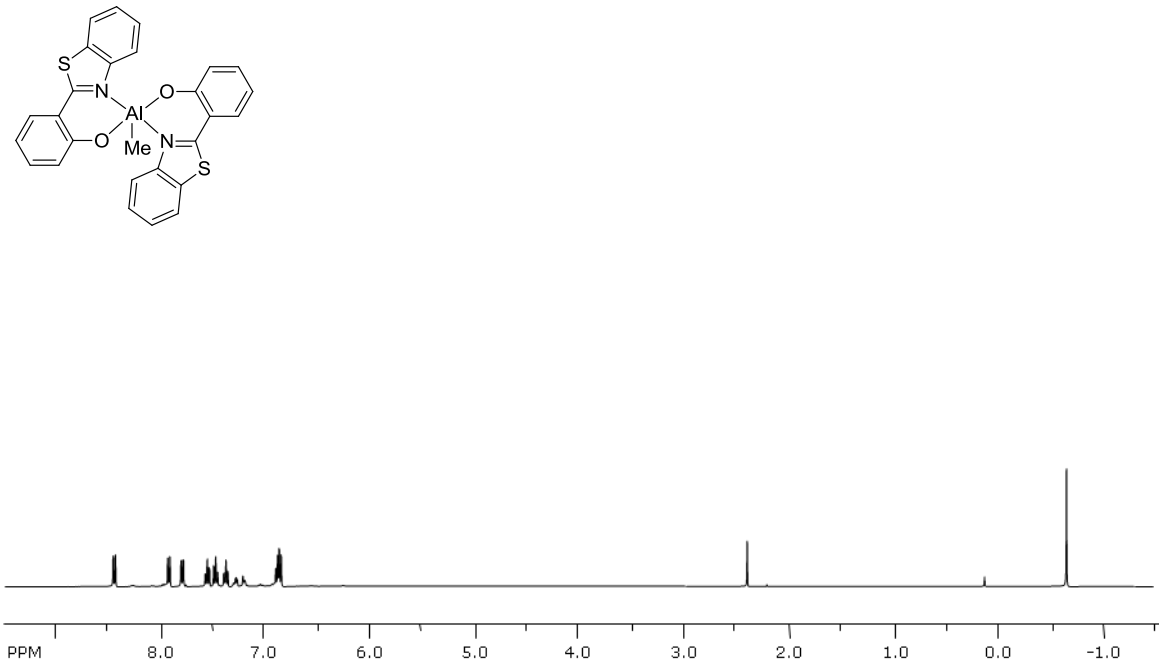

Fig. S8 ^{1}H NMR spectrum of **1b** in $CDCl_3$ at 298 K.

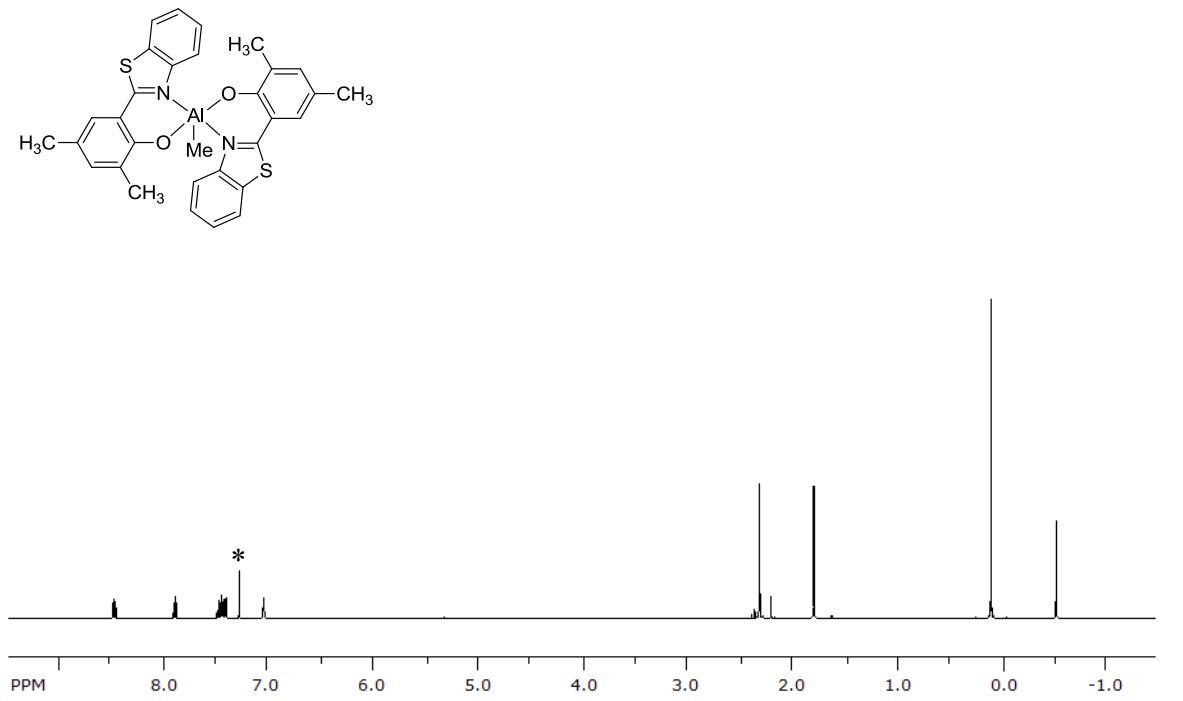

Fig. S9 ^{1}H NMR spectrum of **2b** in $CDCl_3$ at 298 K (* = solvent residue signal).

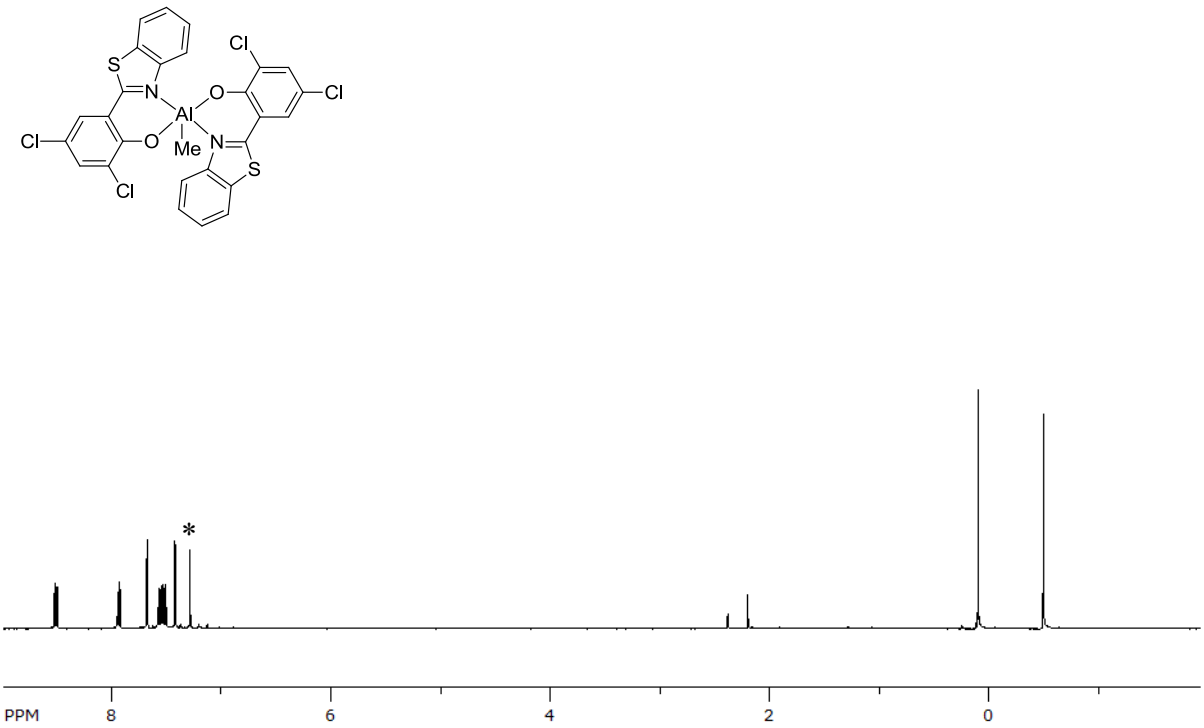

Fig. S10 ^{1}H NMR spectrum of **3b** in $CDCl_3$ at 298 K (* = solvent residue signal).

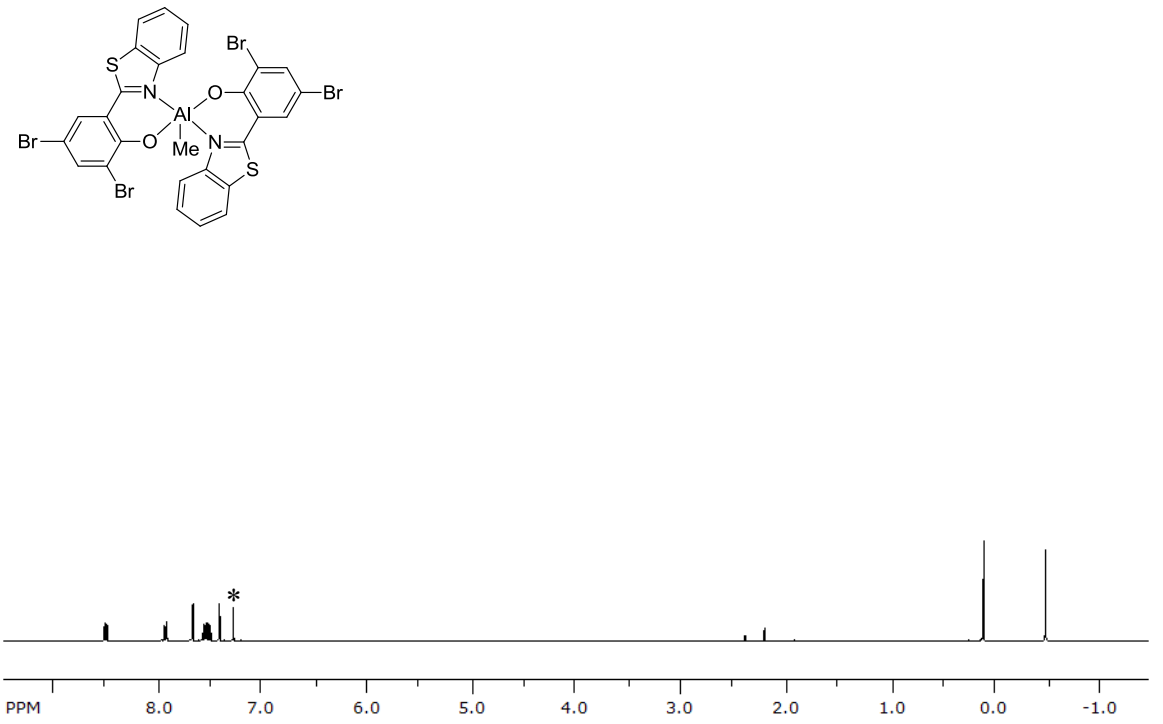

Fig. S11 ^{1}H NMR spectrum of **4b** in $CDCl_3$ at 298 K (* = solvent residue signal).

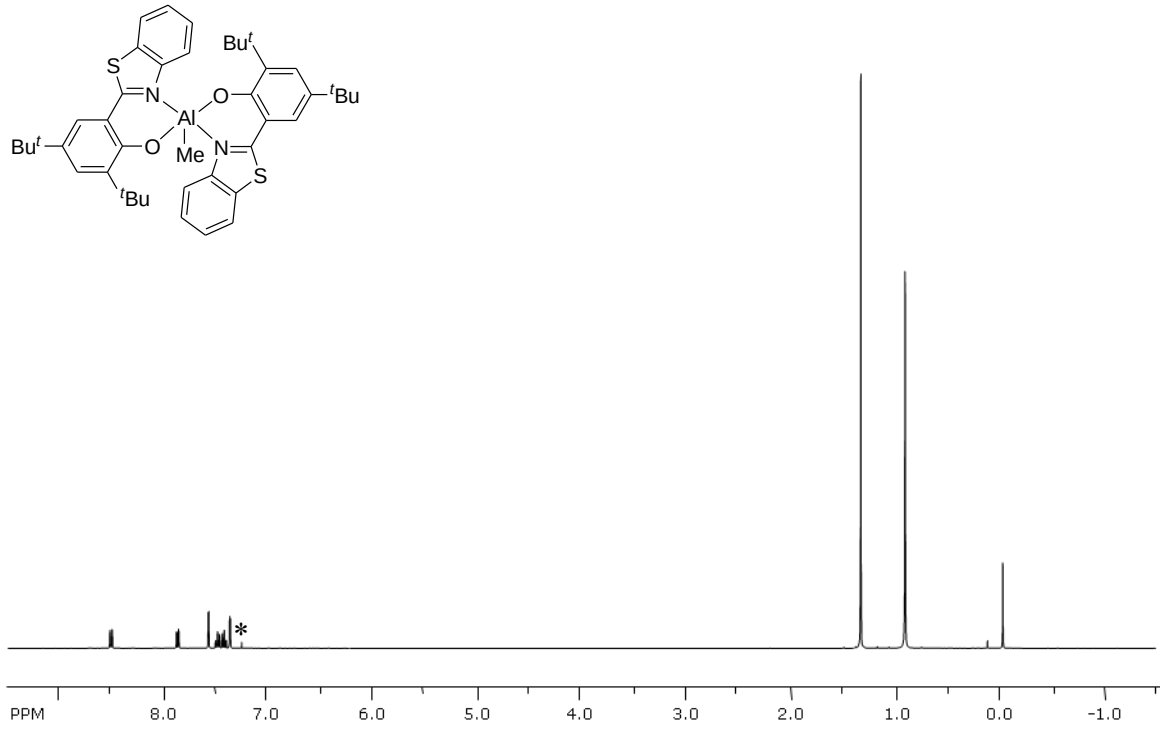

Fig. S12 ^{1}H NMR spectrum of **5b** in $CDCl_3$ at 298 K (* = solvent residue signal).

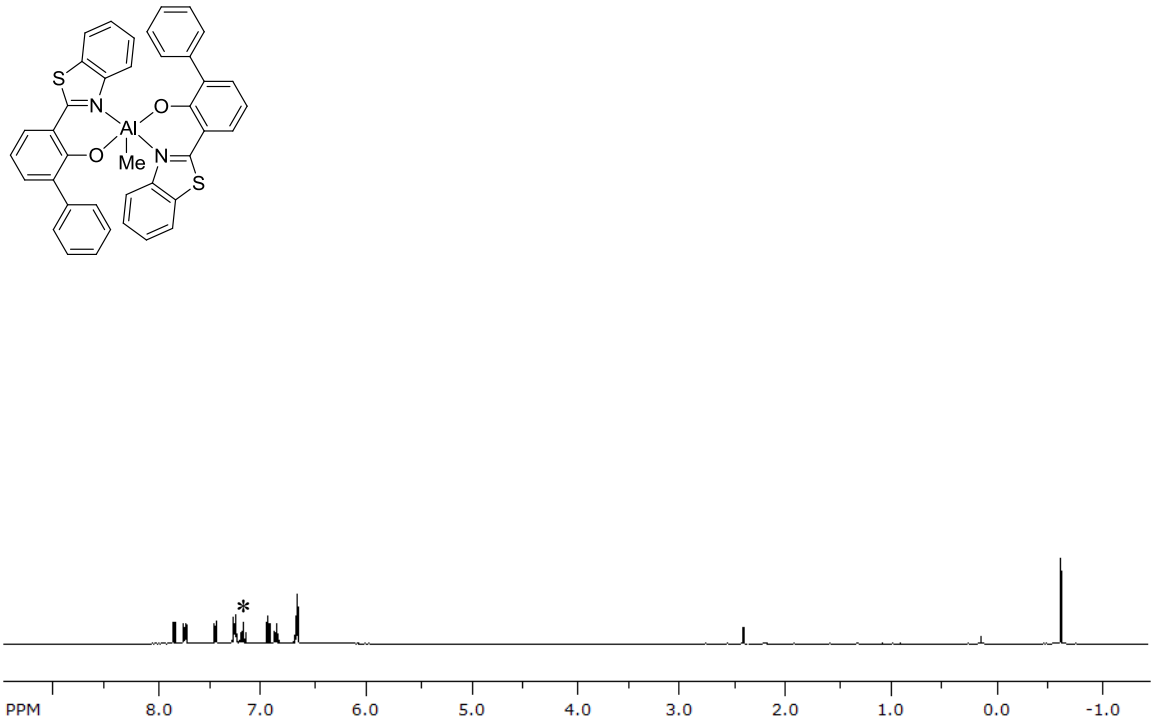

Fig. S13 ^{1}H NMR spectrum of **6b** in $CDCl_3$ at 298 K

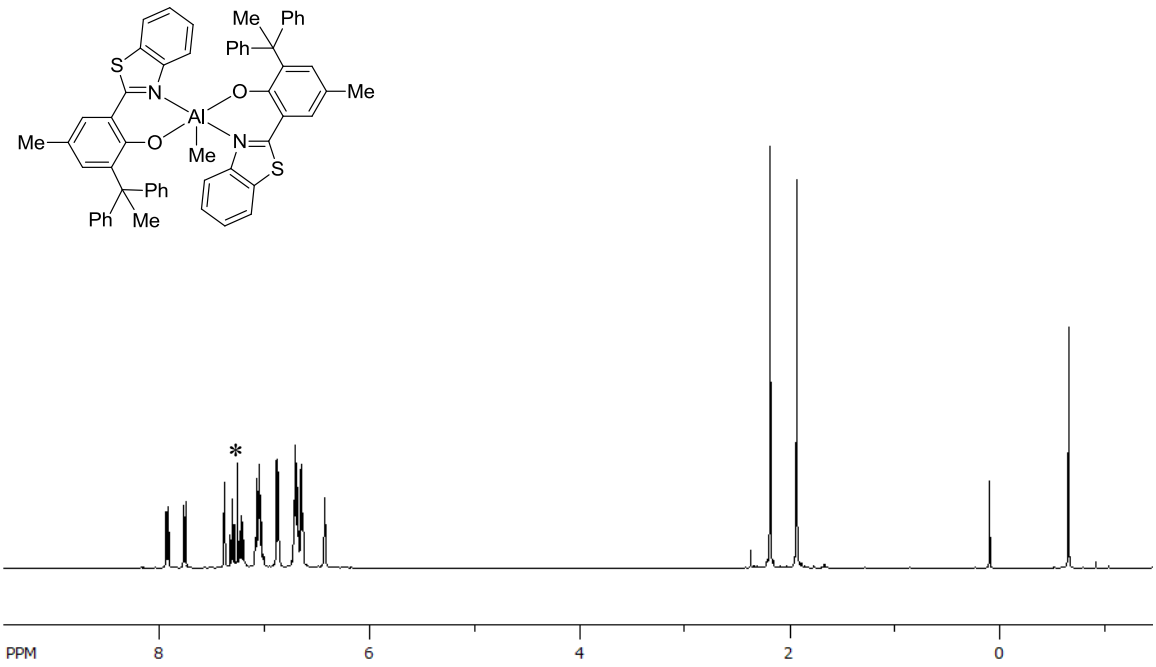

Fig. S14 ^{1}H NMR spectrum of **7b** in $CDCl_3$ at 298 K (* = solvent residue signal).

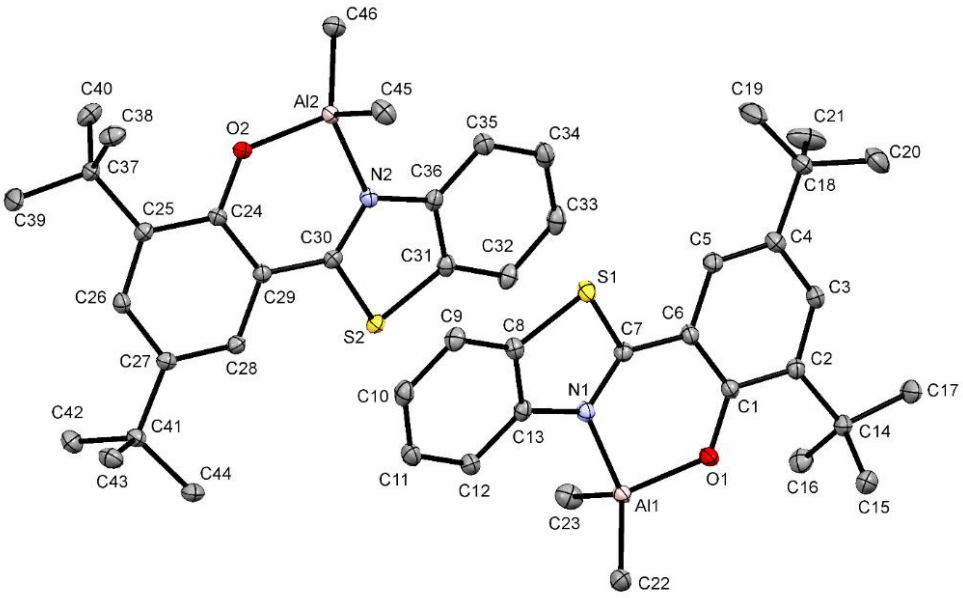

Fig. S15 ORTEP representation of **5a** with the thermal ellipsoids drawn at 50% probability level.

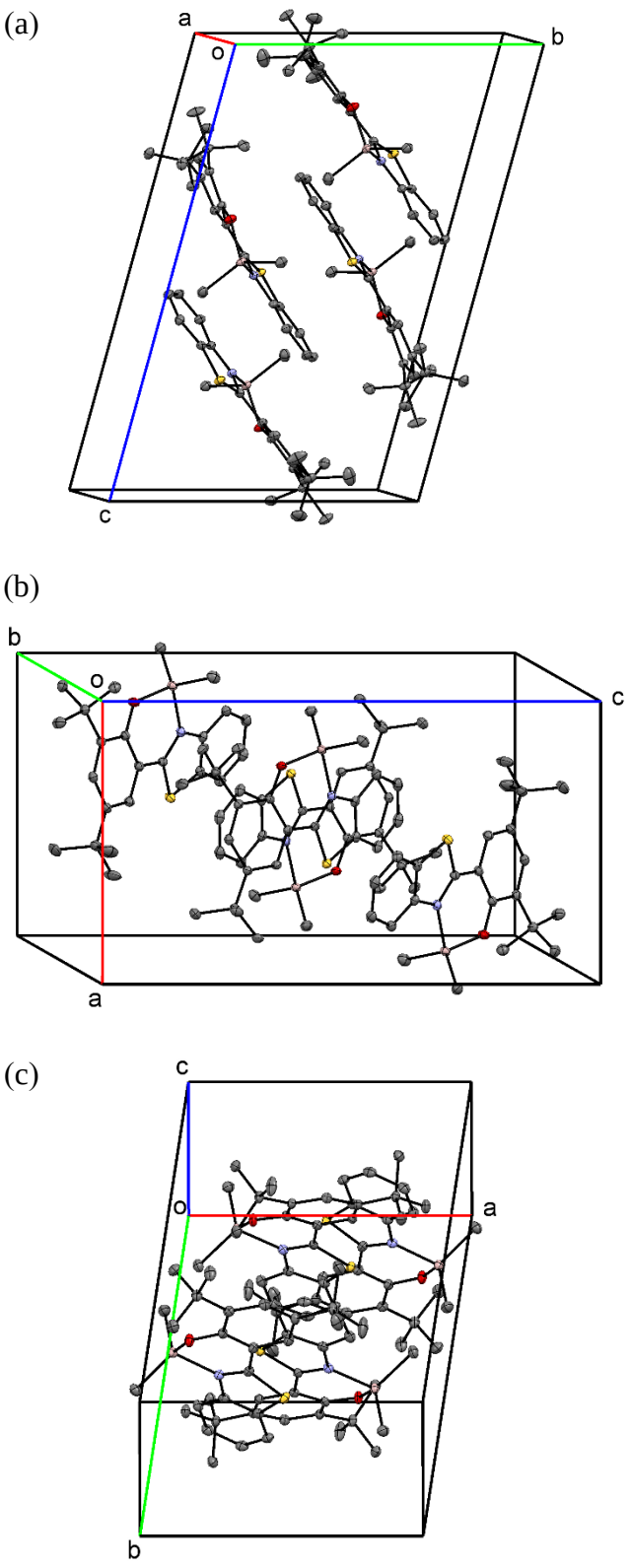

Fig. S16 Stereoview of the unit cell of complex **5a** along (a) a*, (b) b* and (c) c* axes.

Table S1 Crystallographic data and structure refinement details for complex **5a**.

Empirical formula	$C_{23}H_{30}AlNOS$
Formula weight	395.52
Temperature/K	100
Crystal system	triclinic
Space group	P-1
a/Å	10.4459(2)
b/Å	11.9742(3)
c/Å	18.4351(4)
α/°	105.3540(10)
β/°	90.0430(10)
γ/°	98.6420(10)
Volume/Å^3	2196.35(8)
Z	4
ρ_{calc}g/cm^3	1.196
μ/mm^{-1}	1.776
F(000)	848.0
Crystal size/mm^3	0.2 × 0.2 × 0.2
Radiation	CuKα (λ = 1.54178)
2Θ range for data collection/°	7.752 to 149.27
Index ranges	$-13 \leq h \leq 13$, $-14 \leq k \leq 14$, $-23 \leq l \leq 23$
Reflections collected	35972
Independent reflections	8865 [R_{int} = 0.0243, R_{sigma} = 0.0212]
Data/restraints/parameters	8865/0/503
Goodness-of-fit on F^2	1.038
Final R indexes [I>=2σ (I)]	R_1 = 0.0289, wR_2 = 0.0790
Final R indexes [all data]	R_1 = 0.0302, wR_2 = 0.0801
Largest diff. peak/hole / e Å^{-3}	0.30/–0.33

Table S2 Bond lengths (Å) for complex **5a**.

Atom	Atom	Length (Å)	Atom	Atom	Length (Å)
S2	C31	1.7321(11)	C5	C4	1.3740(16)
S2	C30	1.7388(10)	C27	C28	1.3765(15)
S1	C7	1.7420(11)	C27	C26	1.4114(15)
S1	C8	1.7350(11)	C27	C41	1.5321(14)
Al1	O1	1.7712(8)	C28	C29	1.4118(14)
Al1	N1	1.9717(10)	C26	C25	1.3849(15)
Al1	C22	1.9615(12)	C37	C25	1.5398(14)
Al1	C23	1.9555(12)	C37	C40	1.5399(16)
Al2	O2	1.7743(8)	C37	C38	1.5361(15)
Al2	N2	1.9636(10)	C37	C39	1.5351(15)
Al2	C45	1.9649(12)	C4	C3	1.4100(15)
Al2	C46	1.9604(12)	C4	C18	1.5332(15)
O1	C1	1.3282(13)	C29	C30	1.4539(14)
O2	C24	1.3275(13)	C31	C32	1.4005(15)
N2	C36	1.3979(13)	C9	C10	1.3825(16)
N2	C30	1.3263(14)	C9	C8	1.3980(15)
N1	C13	1.3982(13)	C14	C15	1.5381(16)
N1	C7	1.3264(14)	C14	C16	1.5398(16)
C36	C31	1.3997(15)	C14	C17	1.5360(15)
C36	C35	1.3986(15)	C10	C11	1.3997(16)
C6	C5	1.4123(15)	C12	C11	1.3865(16)
C6	C1	1.4162(15)	C33	C32	1.3831(17)
C6	C7	1.4523(15)	C33	C34	1.3975(17)
C24	C25	1.4278(15)	C41	C43	1.5403(15)
C24	C29	1.4167(14)	C41	C42	1.5395(15)
C13	C8	1.3981(15)	C41	C44	1.5328(15)
C13	C12	1.3967(15)	C35	C34	1.3851(16)
C2	C1	1.4273(15)	C18	C20	1.5326(17)
C2	C3	1.3859(15)	C18	C21	1.5323(18)
C2	C14	1.5374(14)	C18	C19	1.5289(17)

Table S3 Bond angles (°) for complex **5a**.

Atom	Atom	Atom	Angle (°)	Atom	Atom	Atom	Angle (°)
C31	S2	C30	90.49(5)	C39	C37	C40	107.19(10)
C8	S1	C7	90.40(5)	C39	C37	C38	107.43(10)
O1	Al1	N1	93.48(4)	C24	C25	C37	120.91(9)
O1	Al1	C22	112.78(5)	C26	C25	C24	117.78(9)
O1	Al1	C23	112.75(5)	C26	C25	C37	121.31(9)
C22	Al1	N1	109.08(5)	C5	C4	C3	116.89(10)
C23	Al1	N1	107.78(5)	C5	C4	C18	123.37(10)
C23	Al1	C22	117.98(5)	C3	C4	C18	119.74(10)
O2	Al2	N2	93.28(4)	C2	C3	C4	124.58(10)
O2	Al2	C45	116.39(5)	C24	C29	C30	120.93(9)
O2	Al2	C46	111.04(5)	C28	C29	C24	120.42(9)
N2	Al2	C45	105.34(5)	C28	C29	C30	118.33(9)
C46	Al2	N2	111.77(5)	C36	C31	S2	109.84(8)
C46	Al2	C45	116.38(5)	C36	C31	C32	121.40(10)
C1	O1	Al1	130.26(7)	C32	C31	S2	128.74(9)
C24	O2	Al2	131.94(7)	C10	C9	C8	117.63(10)
C36	N2	Al2	125.90(7)	N1	C7	S1	113.60(8)
C30	N2	Al2	121.83(7)	N1	C7	C6	125.92(10)
C30	N2	C36	112.24(9)	C6	C7	S1	120.48(8)
C13	N1	Al1	125.95(7)	C2	C14	C15	109.70(9)
C7	N1	Al1	121.61(7)	C2	C14	C16	110.24(9)
C7	N1	C13	112.20(9)	C15	C14	C16	110.49(9)
N2	C36	C31	113.78(10)	C17	C14	C2	111.52(9)
N2	C36	C35	125.82(10)	C17	C14	C15	107.49(9)
C35	C36	C31	120.40(10)	C17	C14	C16	107.35(10)
C5	C6	C1	120.60(10)	C9	C10	C11	121.27(10)
C5	C6	C7	118.22(10)	C13	C8	S1	109.82(8)
C1	C6	C7	121.17(10)	C9	C8	S1	128.80(9)
O2	C24	C25	120.13(9)	C9	C8	C13	121.38(10)
O2	C24	C29	121.25(9)	C11	C12	C13	118.03(10)
C29	C24	C25	118.57(9)	C12	C11	C10	121.17(10)
C8	C13	N1	113.91(9)	C32	C33	C34	121.35(10)
C12	C13	N1	125.59(10)	C27	C41	C43	109.59(9)
C12	C13	C8	120.50(10)	C27	C41	C42	109.55(9)
C1	C2	C14	120.91(9)	C27	C41	C44	111.65(9)
C3	C2	C1	117.74(10)	C42	C41	C43	108.98(9)
C3	C2	C14	121.34(9)	C44	C41	C43	108.55(9)
C4	C5	C6	121.54(10)	C44	C41	C42	108.47(9)
O1	C1	C6	121.12(9)	N2	C30	S2	113.64(8)
O1	C1	C2	120.23(10)	N2	C30	C29	126.29(9)
C6	C1	C2	118.63(10)	C29	C30	S2	119.97(8)
C28	C27	C26	116.76(9)	C33	C32	C31	117.51(11)
C28	C27	C41	123.35(9)	C34	C35	C36	118.02(11)
C26	C27	C41	119.88(9)	C20	C18	C4	109.40(10)
C27	C28	C29	121.64(10)	C21	C18	C4	109.47(10)
C25	C26	C27	124.51(10)	C21	C18	C20	109.38(11)
C25	C37	C40	110.36(9)	C19	C18	C4	111.87(10)
C38	C37	C25	109.95(9)	C19	C18	C20	107.98(11)
C38	C37	C40	110.20(9)	C19	C18	C21	108.69(12)
C39	C37	C25	111.65(9)	C35	C34	C33	121.32(11)

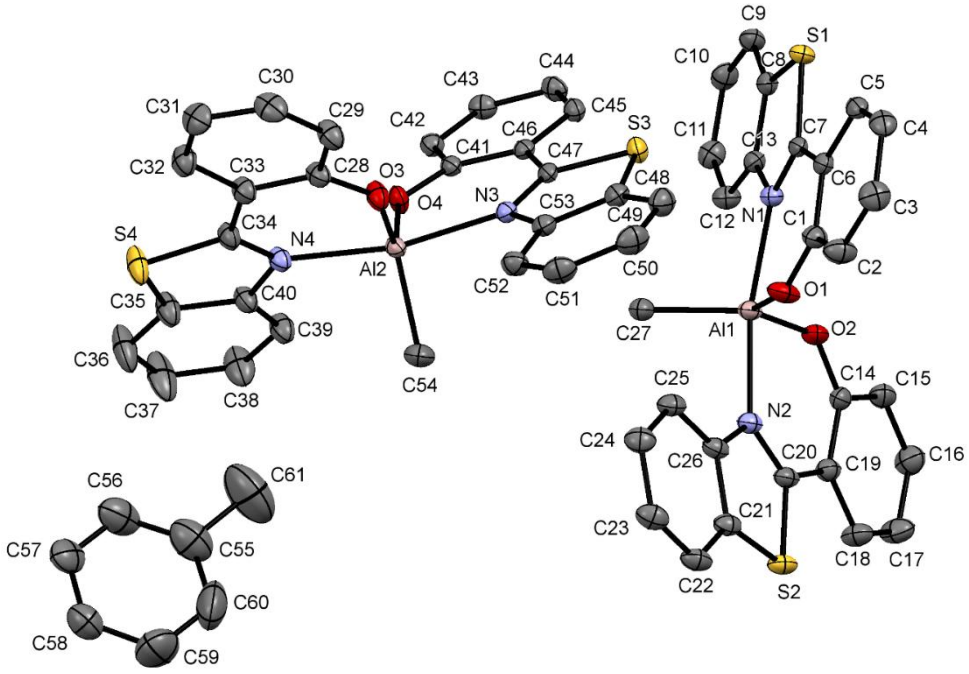

Fig. S17 ORTEP representation of **1b** with the thermal ellipsoids drawn at 50% probability level.

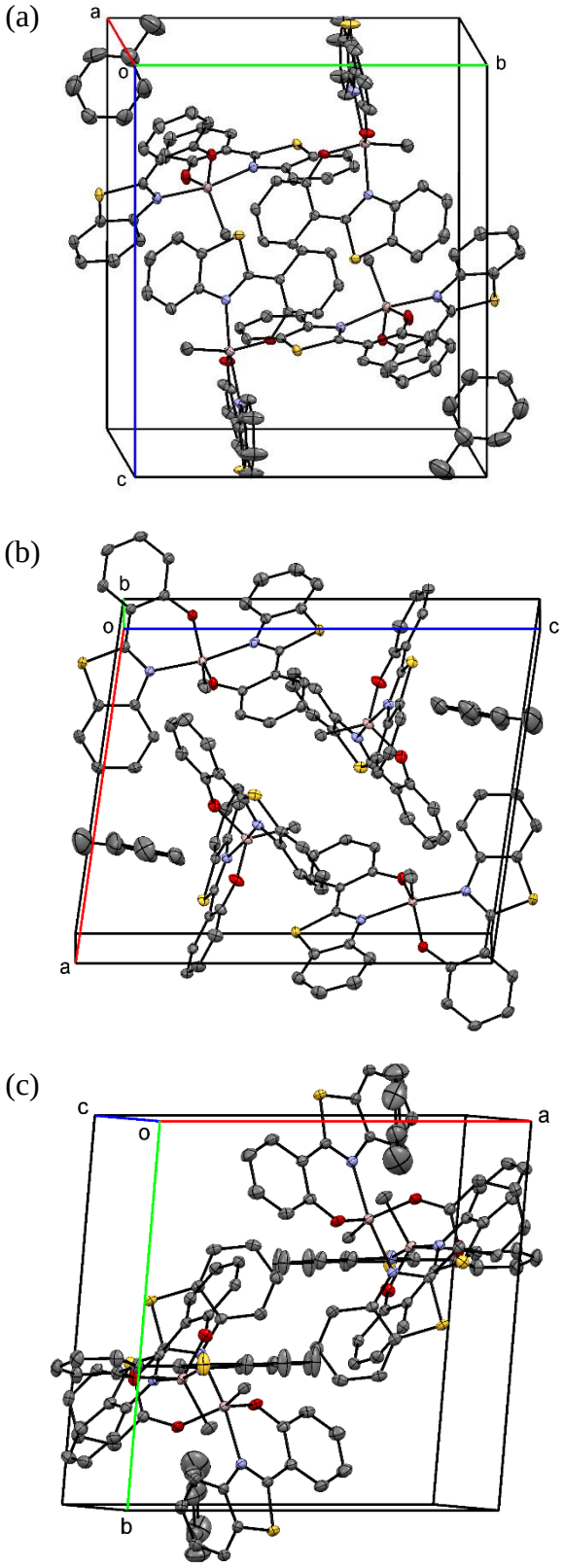

Fig. S18 Stereoview of the unit cell of complex **1b** along (a) a*, (b) b* and (c) c* axes.

Table S4 Crystallographic data and structure refinement details for complex **1b**.

Empirical formula	$C_{30.5}H_{23}AlN_2O_2S_2$
Formula weight	540.61
Temperature/K	100
Crystal system	triclinic
Space group	P-1
a/Å	12.8441(6)
b/Å	13.5123(7)
c/Å	15.8237(8)
α/°	90.0450(10)
β/°	98.2050(10)
γ/°	94.7900(10)
Volume/Å^3	2708.4(2)
Z	4
ρ_{calc}g/cm^3	1.326
μ/mm^{-1}	2.344
F(000)	1124.0
Crystal size/mm^3	0.1 × 0.1 × 0.1
Radiation	CuKα (λ = 1.54178)
2Θ range for data collection/°	8.324 to 144.432
Index ranges	$-15 \le h \le 14$, $-16 \le k \le 16$, $-19 \le l \le 19$
Reflections collected	46865
Independent reflections	10564 [R_{int} = 0.0241, R_{sigma} = 0.0196]
Data/restraints/parameters	10564/0/679
Goodness-of-fit on F^2	1.025
Final R indexes [I>=2σ (I)]	R_1 = 0.0336, wR_2 = 0.0886
Final R indexes [all data]	R_1 = 0.0350, wR_2 = 0.0896
Largest diff. peak/hole / e Å^{-3}	0.79/–0.47

Table S5 Bond lengths (Å) for complex **1b**.

Atom	Atom	Length (Å)	Atom	Atom	Length (Å)
S1	C8	1.7309(15)	C14	C15	1.405(2)
S1	C7	1.7439(14)	C8	C9	1.395(2)
S2	C20	1.7482(14)	C19	C20	1.451(2)
S2	C21	1.7311(16)	C19	C18	1.408(2)
S3	C47	1.7470(14)	C28	C29	1.407(2)
S3	C48	1.7347(15)	C42	C43	1.381(2)
S4	C34	1.7388(16)	C5	C4	1.379(2)
S4	C35	1.7260(17)	C1	C2	1.403(2)
Al2	O4	1.7723(11)	C40	C39	1.398(2)
Al2	O3	1.7729(11)	C40	C35	1.400(2)
Al2	N3	2.0933(13)	C26	C21	1.404(2)
Al2	N4	2.0870(13)	C26	C25	1.401(2)
Al2	C54	1.9656(17)	C45	C44	1.377(2)
Al1	O2	1.7757(12)	C43	C44	1.397(2)
Al1	O1	1.7716(12)	C12	C11	1.381(2)
Al1	N1	2.1125(12)	C52	C51	1.380(2)
Al1	N2	2.0964(13)	C21	C22	1.395(2)
Al1	C27	1.9743(16)	C29	C30	1.377(2)
O4	C41	1.3268(17)	C39	C38	1.380(2)
O2	C14	1.3282(18)	C48	C49	1.398(2)
O3	C28	1.3202(18)	C25	C24	1.383(2)
O1	C1	1.3181(19)	C32	C31	1.377(2)
N1	C13	1.3979(19)	C3	C2	1.380(2)
N1	C7	1.3231(19)	C3	C4	1.394(2)
N3	C53	1.3978(19)	C11	C10	1.402(2)
N3	C47	1.3166(18)	C15	C16	1.380(2)
N4	C34	1.3191(19)	C24	C23	1.405(2)
N4	C40	1.398(2)	C18	C17	1.375(2)
N2	C20	1.315(2)	C9	C10	1.384(2)
N2	C26	1.3991(19)	C30	C31	1.390(3)
C41	C46	1.414(2)	C23	C22	1.381(2)
C41	C42	1.404(2)	C35	C36	1.389(3)
C13	C8	1.405(2)	C51	C50	1.396(3)
C13	C12	1.401(2)	C16	C17	1.393(2)
C33	C28	1.407(2)	C49	C50	1.382(2)
C33	C34	1.451(2)	C36	C37	1.376(3)
C33	C32	1.408(2)	C38	C37	1.399(3)
C46	C47	1.451(2)	C57	C58	1.366(3)
C46	C45	1.409(2)	C57	C56	1.356(3)
C6	C7	1.447(2)	C58	C59	1.363(4)
C6	C5	1.410(2)	C56	C55	1.351(4)
C6	C1	1.411(2)	C55	C60	1.359(4)
C53	C52	1.402(2)	C55	C61	1.514(4)
C53	C48	1.402(2)	C60	C59	1.451(4)
C14	C19	1.415(2)			

Table S6 Bond angles (°) for complex **1b**.

Atom	Atom	Atom	Angle (°)	Atom	Atom	Atom	Angle (°)
C8	S1	C7	90.03(7)	N1	C7	S1	114.48(11)
C21	S2	C20	89.83(7)	N1	C7	C6	125.92(13)
C48	S3	C47	90.07(7)	C6	C7	S1	119.59(11)
C35	S4	C34	89.94(8)	N3	C47	S3	114.23(11)
O4	Al2	O3	119.69(6)	N3	C47	C46	124.95(13)
O4	Al2	N3	88.57(5)	C46	C47	S3	120.82(10)
O4	Al2	N4	88.62(5)	C43	C42	C41	121.44(14)
O4	Al2	C54	119.37(7)	N2	C20	S2	114.43(11)
O3	Al2	N3	83.07(5)	N2	C20	C19	125.63(13)
O3	Al2	N4	88.31(5)	C19	C20	S2	119.94(11)
O3	Al2	C54	120.81(7)	C4	C5	C6	121.58(14)
N4	Al2	N3	168.13(5)	N4	C34	S4	114.71(12)
C54	Al2	N3	94.79(6)	N4	C34	C33	126.02(14)
C54	Al2	N4	96.64(6)	C33	C34	S4	119.27(11)
O2	Al1	N1	87.93(5)	O1	C1	C6	122.74(13)
O2	Al1	N2	89.55(5)	O1	C1	C2	118.48(14)
O2	Al1	C27	118.47(6)	C2	C1	C6	118.78(14)
O1	Al1	O2	119.12(6)	N4	C40	C39	126.27(14)
O1	Al1	N1	87.33(5)	N4	C40	C35	114.17(14)
O1	Al1	N2	83.65(5)	C39	C40	C35	119.55(15)
O1	Al1	C27	122.35(6)	N2	C26	C21	113.82(13)
N2	Al1	N1	167.99(5)	N2	C26	C25	126.75(13)
C27	Al1	N1	97.09(6)	C25	C26	C21	119.42(14)
C27	Al1	N2	94.43(6)	C44	C45	C46	121.72(14)
C41	O4	Al2	136.19(10)	C42	C43	C44	120.35(14)
C14	O2	Al1	135.05(10)	C45	C44	C43	119.10(13)
C28	O3	Al2	137.84(10)	C11	C12	C13	118.76(14)
C1	O1	Al1	138.79(10)	C51	C52	C53	118.46(15)
C13	N1	Al1	123.99(10)	C26	C21	S2	110.06(11)
C7	N1	Al1	124.37(10)	C22	C21	S2	128.17(12)
C7	N1	C13	111.45(12)	C22	C21	C26	121.76(14)
C53	N3	Al2	122.83(9)	C30	C29	C28	120.84(16)
C47	N3	Al2	125.27(10)	C38	C39	C40	118.21(15)
C47	N3	C53	111.84(12)	C53	C48	S3	109.63(11)
C34	N4	Al2	124.16(11)	C49	C48	S3	128.60(12)
C34	N4	C40	111.17(13)	C49	C48	C53	121.76(14)
C40	N4	Al2	124.36(10)	C24	C25	C26	118.79(14)
C20	N2	Al1	123.87(10)	C31	C32	C33	121.33(16)
C20	N2	C26	111.86(12)	C2	C3	C4	120.31(15)
C26	N2	Al1	124.11(10)	C12	C11	C10	121.22(15)
O4	C41	C46	123.59(13)	C3	C2	C1	121.24(15)
O4	C41	C42	118.05(13)	C16	C15	C14	121.71(15)
C42	C41	C46	118.36(13)	C5	C4	C3	119.28(14)
N1	C13	C8	114.19(13)	C25	C24	C23	121.16(15)
N1	C13	C12	126.34(13)	C17	C18	C19	121.74(15)
C12	C13	C8	119.48(13)	C10	C9	C8	117.91(14)
C28	C33	C34	120.33(13)	C29	C30	C31	120.68(15)
C28	C33	C32	119.05(14)	C22	C23	C24	120.76(15)
C32	C33	C34	120.62(14)	C23	C22	C21	118.10(14)
C41	C46	C47	120.76(12)	C32	C31	C30	119.25(15)

Atom	Atom	Atom	Angle (°)	Atom	Atom	Atom	Angle (°)
C45	C46	C41	119.00(13)	C40	C35	S4	109.94(12)
C45	C46	C47	120.24(13)	C36	C35	S4	127.73(14)
C5	C6	C7	120.88(13)	C36	C35	C40	122.33(16)
C5	C6	C1	118.77(13)	C9	C10	C11	120.85(14)
C1	C6	C7	120.35(13)	C52	C51	C50	121.45(15)
N3	C53	C52	126.19(14)	C15	C16	C17	120.54(16)
N3	C53	C48	114.22(13)	C18	C17	C16	118.91(16)
C48	C53	C52	119.58(14)	C50	C49	C48	117.68(15)
O2	C14	C19	123.50(14)	C49	C50	C51	121.07(15)
O2	C14	C15	118.76(13)	C37	C36	C35	117.12(17)
C15	C14	C19	117.74(14)	C39	C38	C37	121.20(17)
C13	C8	S1	109.85(11)	C56	C57	C58	122.1(2)
C9	C8	S1	128.39(12)	C59	C58	C57	119.0(2)
C9	C8	C13	121.77(14)	C36	C37	C38	121.55(18)
C14	C19	C20	121.04(13)	C55	C56	C57	121.2(2)
C18	C19	C14	119.36(14)	C56	C55	C60	119.2(2)
C18	C19	C20	119.60(14)	C56	C55	C61	120.8(3)
O3	C28	C33	122.81(14)	C60	C55	C61	120.0(3)
O3	C28	C29	118.55(14)	C55	C60	C59	120.1(2)
C33	C28	C29	118.64(14)	C58	C59	C60	118.4(2)

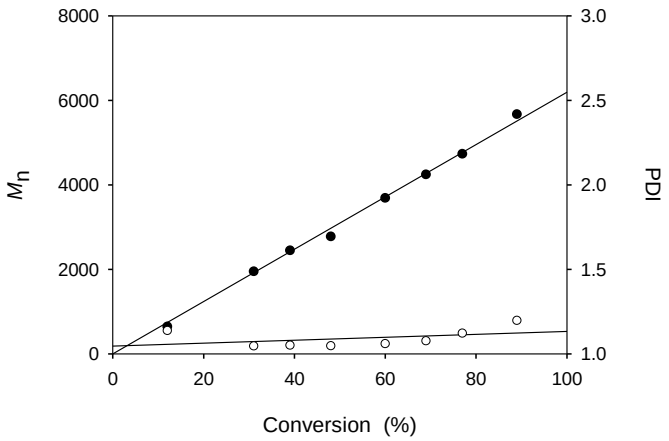

Fig. S19 Plot of the PLA M_n (●) (*versus* polystyrene standards) and PDI (○) as a function of monomer conversion for *rac*-LA using **1a**/$PhCH_2OH$ as an initiator ($[LA]_0/[Al]$ = 50, toluene, 70 °C).

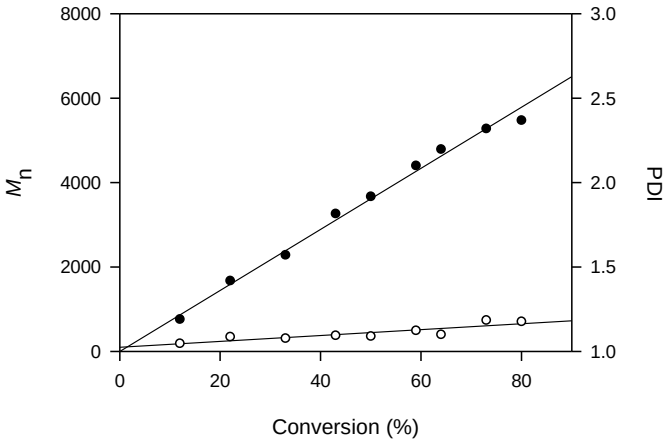

Fig. S20 Plot of the PLA M_n (●) (*versus* polystyrene standards) and PDI (○) as a function of monomer conversion for *rac*-LA using **2a**/$PhCH_2OH$ as an initiator ($[LA]_0/[Al]$ = 50, toluene, 70 °C).

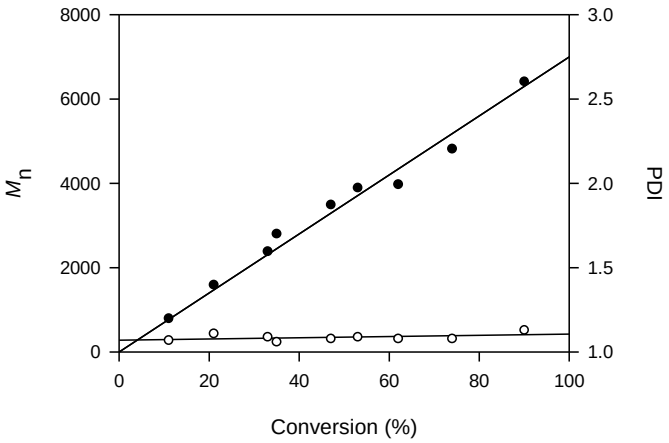

Fig. S21 Plot of the PLA M_n (●) (*versus* polystyrene standards) and PDI (○) as a function of monomer conversion for *rac*-LA using **4a**/$PhCH_2OH$ as an initiator ($[LA]_0/[Al]$ = 50, toluene, 70 °C).

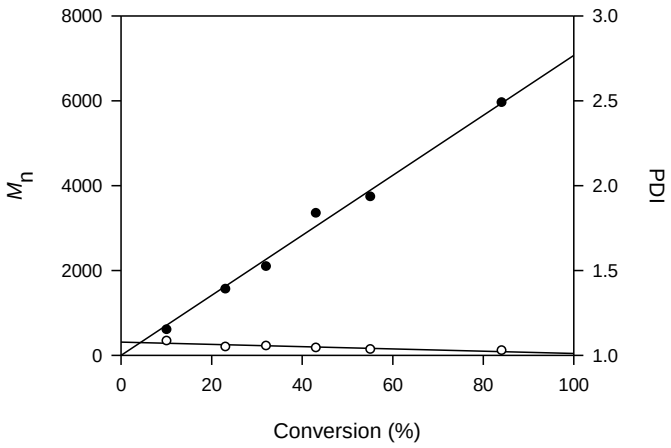

Fig. S22 Plot of the PLA M_n (●) (*versus* polystyrene standards) and PDI (○) as a function of monomer conversion for *rac*-LA using **5a**/$PhCH_2OH$ as an initiator ($[LA]_0/[Al]$ = 50, toluene, 70 °C).

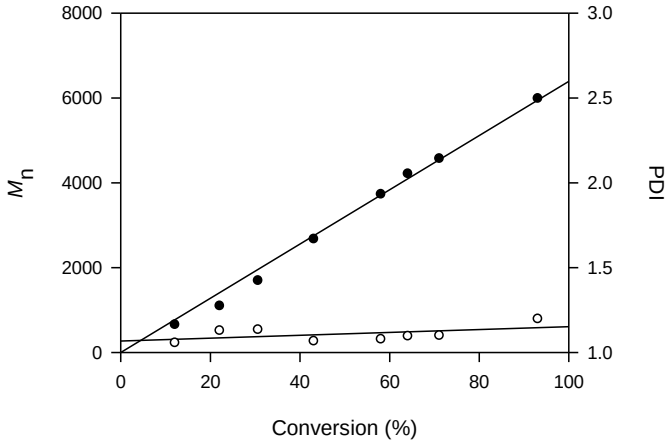

Fig. S23 Plot of the PLA M_n (●) (*versus* polystyrene standards) and PDI (○) as a function of monomer conversion for *rac*-LA using **6a**/$PhCH_2OH$ as an initiator ($[LA]_0/[Al]$ = 50, toluene, 70 °C).

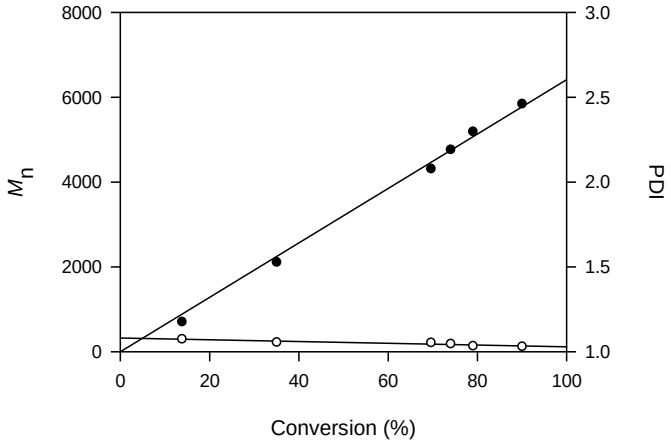

Fig. S24 Plot of the PLA M_n (●) (*versus* polystyrene standards) and PDI (○) as a function of monomer conversion for *rac*-LA using **7a**/$PhCH_2OH$ as an initiator ($[LA]_0/[Al]$ = 50, toluene, 70 °C).

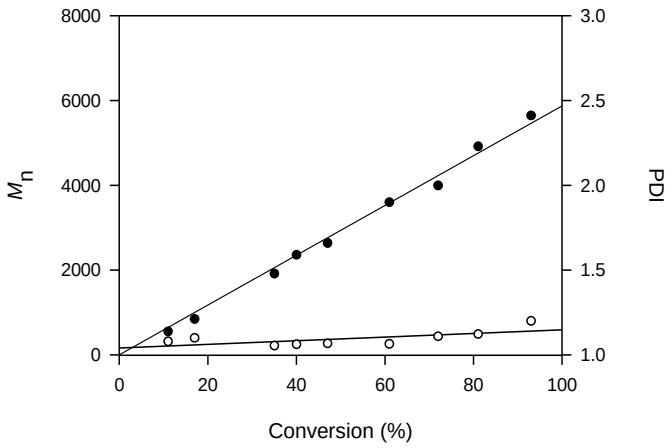

Fig. S25 Plot of the PLA M_n (●) (*versus* polystyrene standards) and PDI (○) as a function of monomer conversion for *rac*-LA using **1b**/$PhCH_2OH$ as an initiator ($[LA]_0/[Al]$ = 50, toluene, 70 °C).

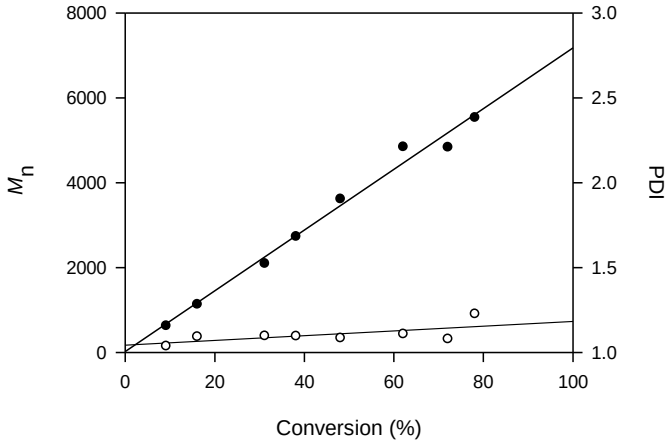

Fig. S26 Plot of the PLA M_n (●) (*versus* polystyrene standards) and PDI (○) as a function of monomer conversion for *rac*-LA using **2b**/$PhCH_2OH$ as an initiator ($[LA]_0/[Al]$ = 50, toluene, 70 °C).

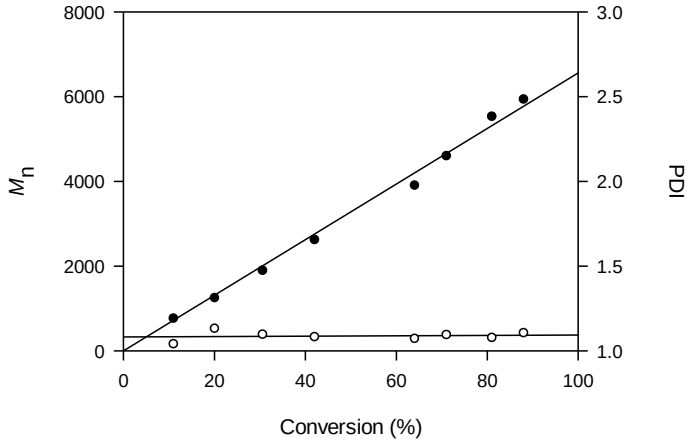

Fig. S27 Plot of the PLA M_n (●) (*versus* polystyrene standards) and PDI (○) as a function of monomer conversion for *rac*-LA using **3b**/$PhCH_2OH$ as an initiator ($[LA]_0/[Al]$ = 50, toluene, 70 °C).

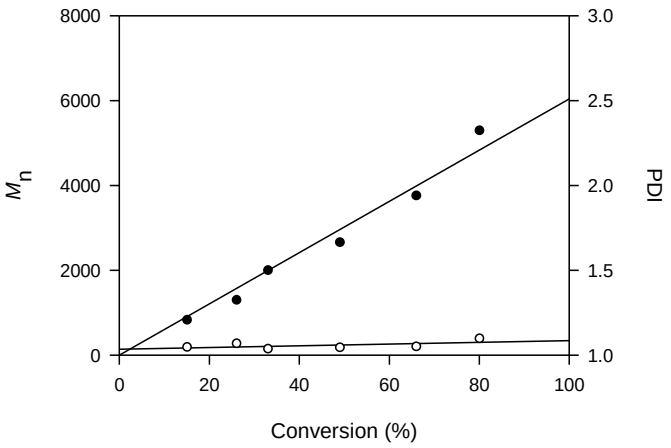

Fig. S28 Plot of the PLA M_n (●) (*versus* polystyrene standards) and PDI (○) as a function of monomer conversion for *rac*-LA using **4b**/$PhCH_2OH$ as an initiator ($[LA]_0/[Al]$ = 50, toluene, 70 °C).

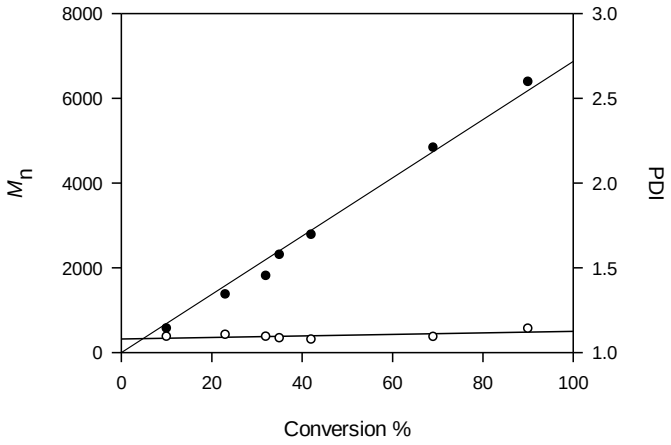

Fig. S29 Plot of the PLA M_n (●) (*versus* polystyrene standards) and PDI (○) as a function of monomer conversion for *rac*-LA using **5b**/$PhCH_2OH$ as an initiator ($[LA]_0/[Al]$ = 50, toluene, 70 °C).

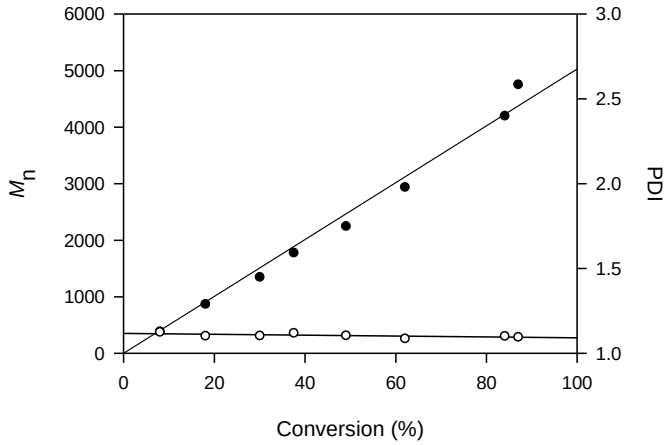

Fig. S30 Plot of the PLA M_n (●) (*versus* polystyrene standards) and PDI (○) as a function of monomer conversion for *rac*-LA using **6b**/$PhCH_2OH$ as an initiator ($[LA]_0/[Al]$ = 50, toluene, 70 °C).

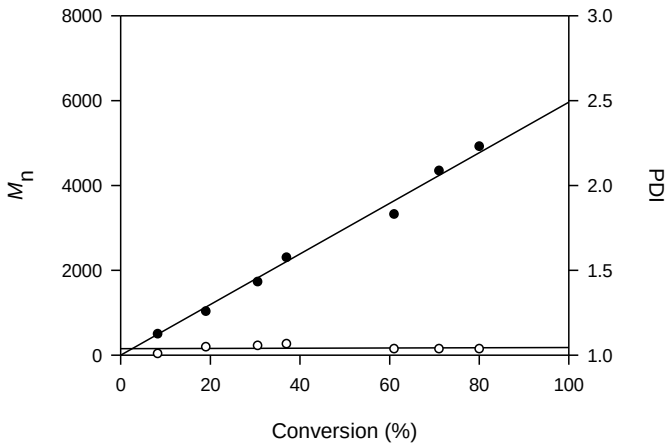

Fig. S31 Plot of the PLA M_n (●) (*versus* polystyrene standards) and PDI (○) as a function of monomer conversion for *rac*-LA using **7b**/$PhCH_2OH$ as an initiator ($[LA]_0/[Al] = 50$, toluene, 70 °C).

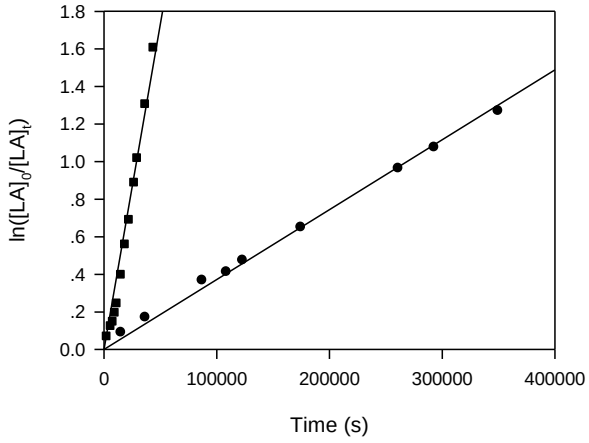

Fig. S32 Semilogarithmic plots of the *rac*-lactide conversion *versus* time in toluene at 70 °C with complexes **2a** (■) and **2b** (●) ($[LA]_0/[Al]/[PhCH_2OH] = 50:1:1$, $[LA]_0 = 0.42$ M, [Al] = 8.33 mM).

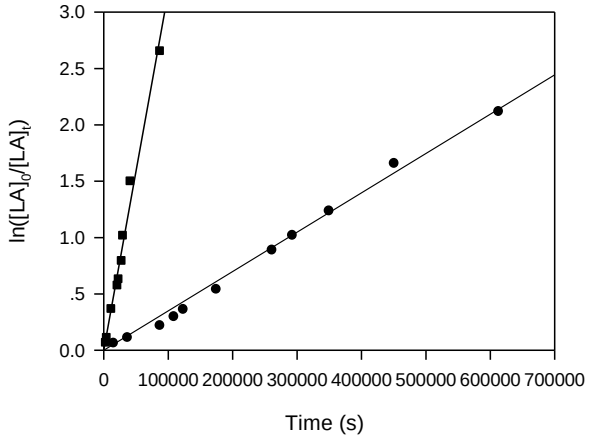

Fig. S33 Semilogarithmic plots of the *rac*-lactide conversion *versus* time in toluene at 70 °C with complexes **3a** (■) and **3b** (●)($[LA]_0/[Al]/[PhCH_2OH] = 50:1:1$, $[LA]_0 = 0.42$ M, [Al] = 8.33 mM).

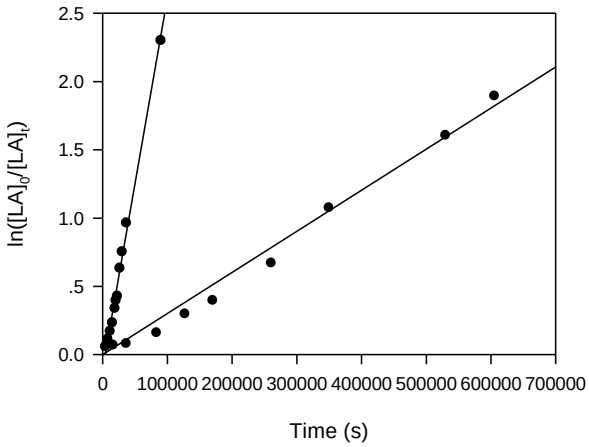

Fig. S34 Semilogarithmic plots of the *rac*-lactide conversion *versus* time in toluene at 70 °C with complexs **4a** (■) and **4b** (●) ($[LA]_0/[Al]/[PhCH_2OH]$ = 50:1:1, $[LA]_0$ = 0.42 M, [Al] = 8.33 mM).

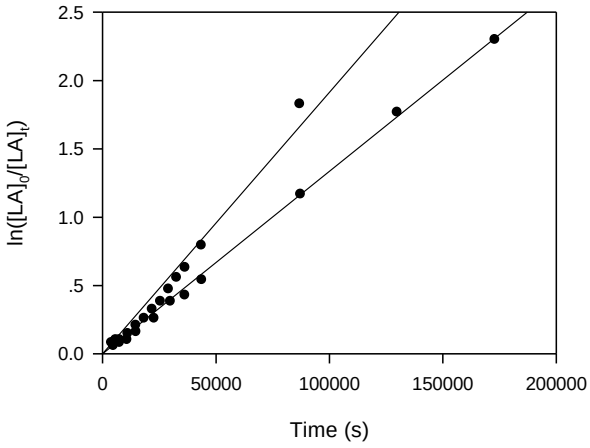

Fig. S35 Semilogarithmic plots of the *rac*-lactide conversion *versus* time in toluene at 70 °C with complexs **5a** (■) and **5b** (●) ($[LA]_0/[Al]/[PhCH_2OH]$ = 50:1:1, $[LA]_0$ = 0.42 M, [Al] = 8.33 mM).

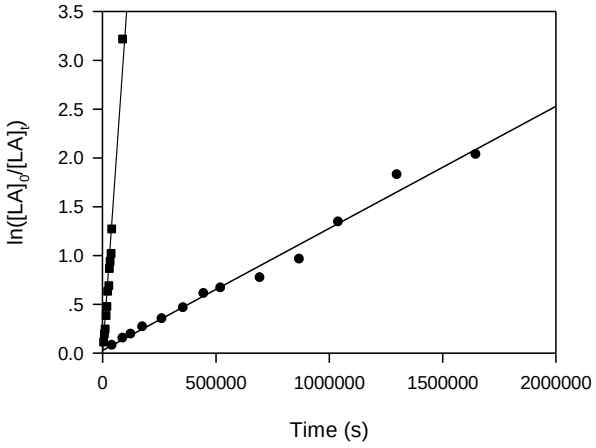

Fig. S36 Semilogarithmic plots of the *rac*-lactide conversion *versus* time in toluene at 70 °C with complexs **6a** (■) and **6b** (●) ($[LA]_0/[Al]/[PhCH_2OH]$ = 50:1:1, $[LA]_0$ = 0.42 M, [Al] = 8.33 mM).

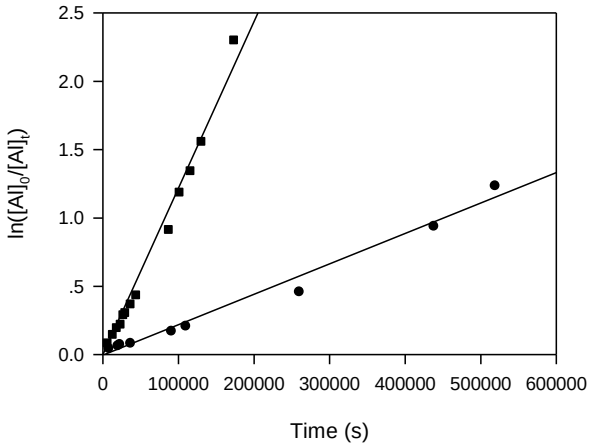

Fig. S37 Semilogarithmic plots of the *rac*-lactide conversion *versus* time in toluene at 70 °C with complexs **7a** (■) and **7b** (●) ($[LA]_0/[Al]/[PhCH_2OH]$ = 50:1:1, $[LA]_0$ = 0.42 M, [Al] = 8.33 mM).

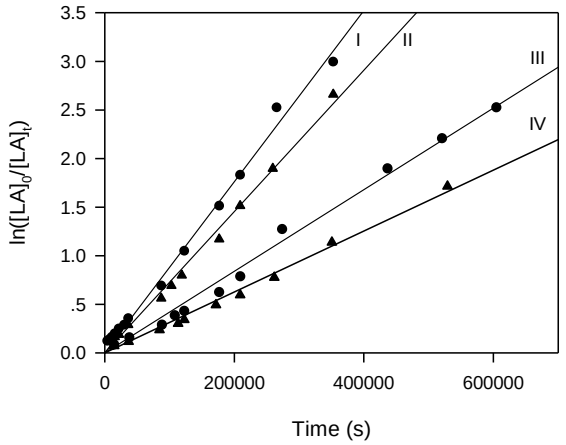

Fig. S38 Semilogarithmic plots of the *rac*-lactide conversion *versus* time in toluene at 70 °C with complex **1b**/$PhCH_2OH$ as an initiator ($[LA]_0$ = 0.42 M: **I**, [Al] = 25 mM, $[LA]_0/[Al]$ = 17; **II**,[Al] = 20.80 mM, $[LA]_0/[Al]$ = 20; **III**, [Al] = 16.67 mM, $[LA]_0/[Al]$ = 25; I**V**, [Al] = 12.50 mM, $[LA]_0/[Al]$ = 34).

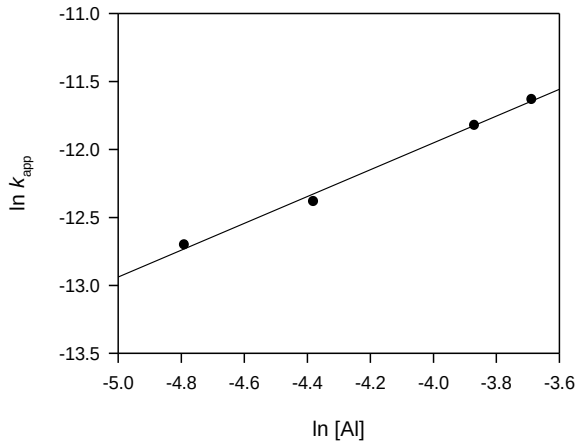

Fig. S39 Plot of ln k_{app} versus ln [Al] for the polymerisation of *rac*-lactide with complex **1b**/$PhCH_2OH$ as an initiator (toluene, 70 °C, $[LA]_0$ = 0.42 M).

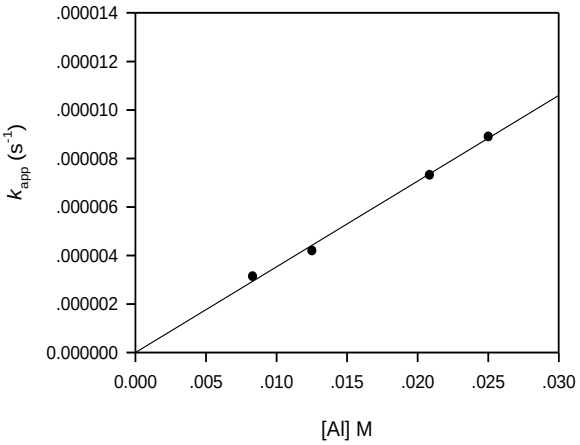

Fig. S40 Plot of k_{app} versus [Al] for the polymerisation of *rac*-lactide with complex **1b**/$PhCH_2OH$ as an initiator (toluene, 70 °C, $[LA]_0$ = 0.42 M).

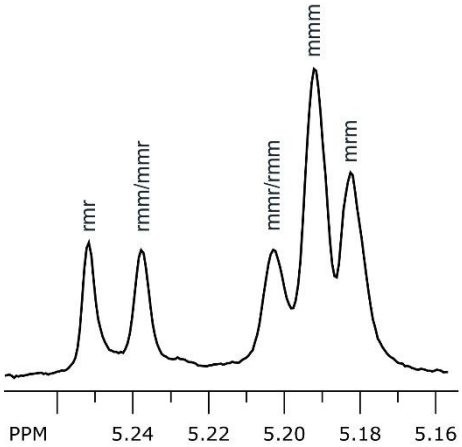

Fig. S41 Homonuclear decoupled ^1H NMR spectrum of the methine region of PLA prepared from *rac*-lactide at 70 °C in toluene (400 MHz, $CDCl_3$) with **1a**/$PhCH_2OH$.

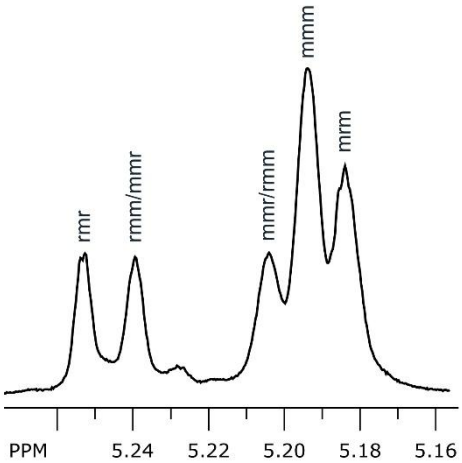

Fig. S42 Homonuclear decoupled ^1H NMR spectrum of the methine region of PLA prepared from *rac*-lactide at 70˚C in toluene (400 MHz, $CDCl_3$) with **2a**/$PhCH_2OH$.

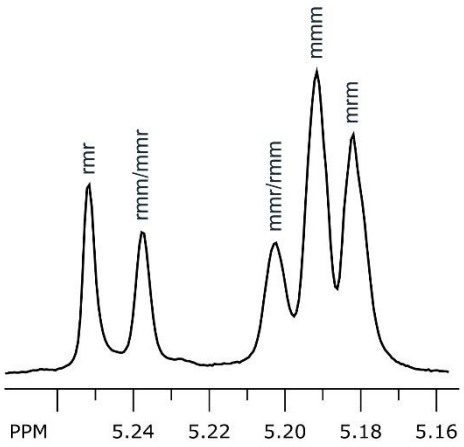

Fig. S43 Homonuclear decoupled ^{1}H NMR spectrum of the methine region of PLA prepared from *rac*-lactide at 70 °C in toluene (400 MHz, $CDCl_3$) with **3a**/$PhCH_2OH$.

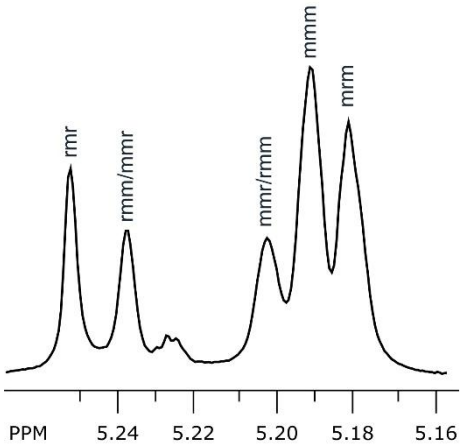

Fig. S44 Homonuclear decoupled ^{1}H NMR spectrum of the methine region of PLA prepared from *rac*-lactide at 70 °C in toluene (400 MHz, $CDCl_3$) with **4a**/$PhCH_2OH$.

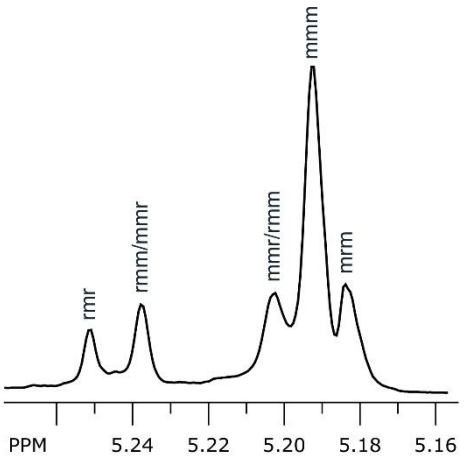

Fig. S45 Homonuclear decoupled ^{1}H NMR spectrum of the methine region of PLA prepared from *rac*-lactide at 70 °C in toluene (400 MHz, $CDCl_3$) with **5a**/$PhCH_2OH$.

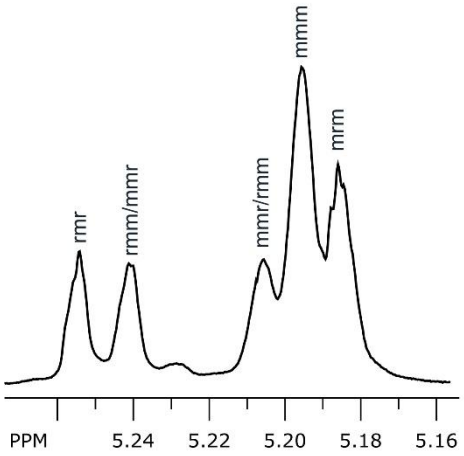

Fig. S46 Homonuclear decoupled ^{1}H NMR spectrum of the methine region of PLA prepared from *rac*-lactide at 70 °C in toluene (400 MHz, $CDCl_3$) with **6a**/$PhCH_2OH$.

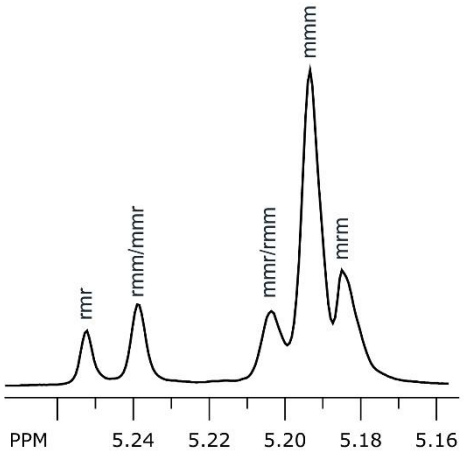

Fig. S47 Homonuclear decoupled ^{1}H NMR spectrum of the methine region of PLA prepared from *rac*-lactide at 70 °C in toluene (400 MHz, $CDCl_3$) with **7a**/$PhCH_2OH$.

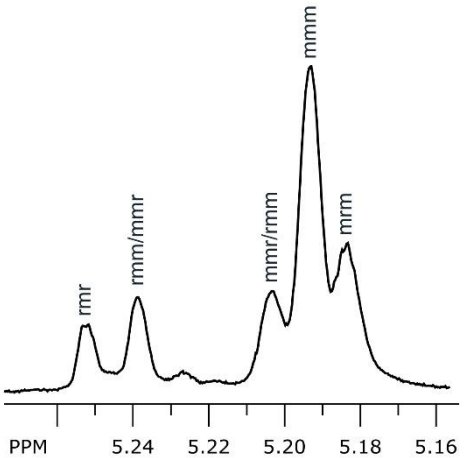

Fig. S48 Homonuclear decoupled ^{1}H NMR spectrum of the methine region of PLA prepared from *rac*-lactide at 70 °C in toluene (400 MHz, $CDCl_3$) with **1b**/$PhCH_2OH$.

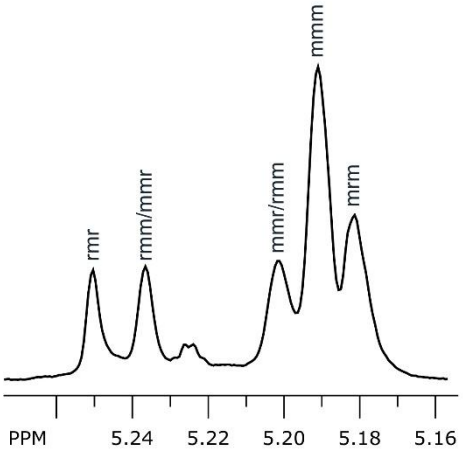

Fig. S49 Homonuclear decoupled ^{1}H NMR spectrum of the methine region of PLA prepared from *rac*-lactide at 70 °C in toluene (400 MHz, $CDCl_3$) with **2b**/$PhCH_2OH$.

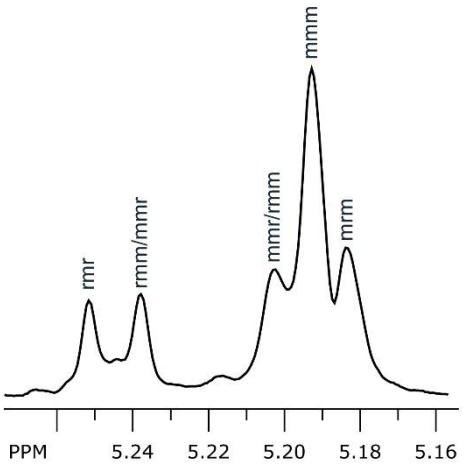

Fig. S50 Homonuclear decoupled ^{1}H NMR spectrum of the methine region of PLA prepared from *rac*-lactide at 70 °C in toluene (400 MHz, $CDCl_3$) with **3b**/$PhCH_2OH$.

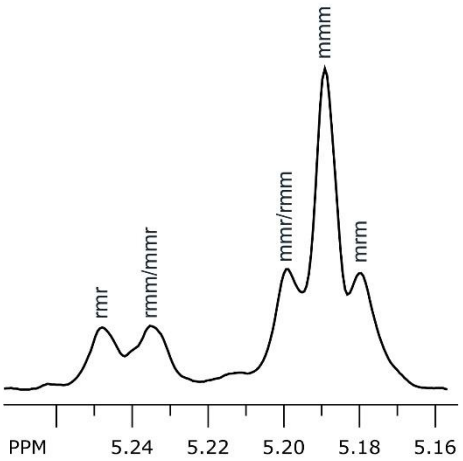

Fig. S51 Homonuclear decoupled ^{1}H NMR spectrum of the methine region of PLA prepared from *rac*-lactide at 70 °C in toluene (400 MHz, $CDCl_3$) with **4b**/$PhCH_2OH$.

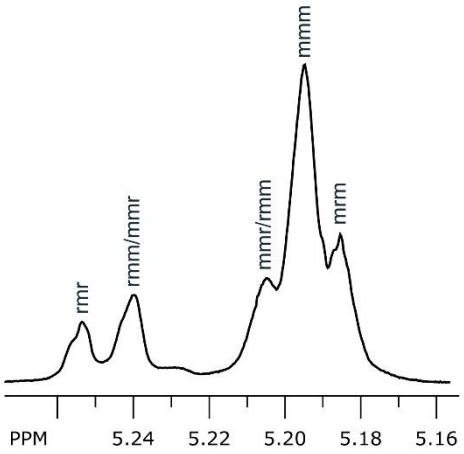

Fig. S52 Homonuclear decoupled ^{1}H NMR spectrum of the methine region of PLA prepared from *rac*-lactide at 70 °C in toluene (400 MHz, $CDCl_3$) with **5b**/$PhCH_2OH$.

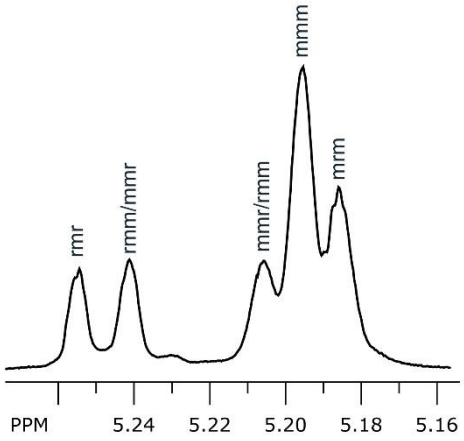

Fig. S53 Homonuclear decoupled ^{1}H NMR spectrum of the methine region of PLA prepared from *rac*-lactide at 70 °C in toluene (400 MHz, $CDCl_3$) with **6b**/$PhCH_2OH$.

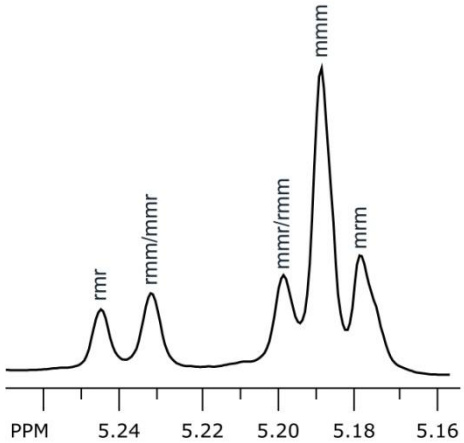

Fig. S54 Homonuclear decoupled ^{1}H NMR spectrum of the methine region of PLA prepared from *rac*-lactide at 70 °C in toluene (400 MHz, $CDCl_3$) with **7b**/$PhCH_2OH$.

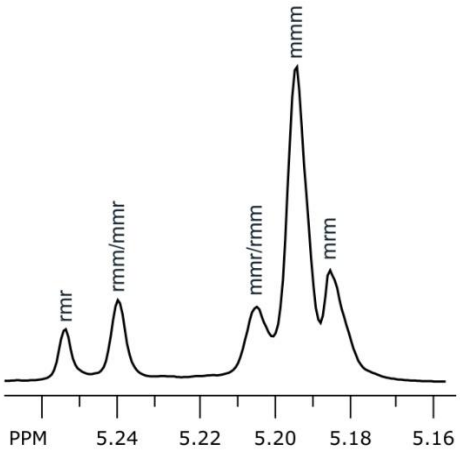

Fig. S55 Homonuclear decoupled ^{1}H NMR spectrum of the methine region of PLA prepared from *rac*-lactide at 50 °C in toluene (400 MHz, $CDCl_3$) with **5a**/ $PhCH_2OH$.

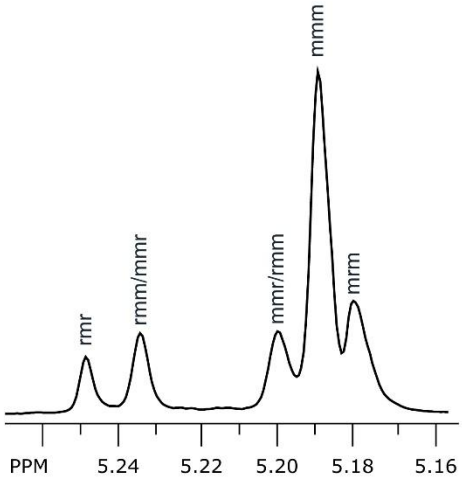

Fig. S56 Homonuclear decoupled ^{1}H NMR spectrum of the methine region of PLA prepared from *rac*-lactide at 50 °C in toluene (400 MHz, $CDCl_3$) with **7a**/ $PhCH_2OH$.

Table S7 Selected structural parameters of the optimized structures of complexes **1a** and **1a′**.

Complex 1a		**Complex 1a′**	
Bond distance	**Å**	**Bond distance**	**Å**
C1–Al	1.960	C1–Al	1.959
C2–Al	1.962	C2–Al	1.959
O1–Al	1.796	O1–Al	1.802
N1–Al	2.002	N1–Al	1.991
C3–N1	1.315	C3–N1	1.314
C3–O2	1.752	C3–S1	1.348
C3–C4	1.450	C3–C4	1.437
C4–C5	1.422	C4–C5	1.421
C5–O1	1.307	C5–O1	1.306
C6–O2	1.740	C6–S1	1.371
C6–C7	1.399	C6–C7	1.388
C7–N1	1.391	C7–N1	1.395
Bond angle	**degrees**	**Bond angle**	**degrees**
C1–Al–C2	121.4	C1–Al–C2	120.7
C1–Al–O1	113.7	C1–Al–O1	113.2
C1–Al–N1	105.3	C1–Al–N1	107.0
C2–Al–O1	111.9	C2–Al–O1	113.5
C2–Al–N1	108.0	C2–Al–N1	106.4
O1–Al–N1	91.8	O1–Al–N1	91.2
C3–N1–C7	113.2	C3–N1–C7	106.4
C4–O2–C6	90.2	C4–S1–C6	106.1

Table S8 Selected structural parameters of the optimized structures of complexes **1b** and **1b′**.

Complex 1b		**Complex 1b′**	
Bond distance	**Å**	**Bond distance**	**Å**
C1–Al	1.971	C1–Al	1.969
O1–Al	1.794	O1–Al	1.815
O3–Al	1.791	O2–Al	1.815
N1–Al	2.097	N1–Al	2.041
N2–Al	2.084	N2–Al	2.047
C2–N1	1.308	C2–N1	1.306
C2–O2	1.754	C2–S1	1.351
C2–C3	1.454	C2–C3	1.439
C3–C4	1.416	C3–C4	1.417
C4–O1	1.310	C4–O1	1.311
C5–O2	1.737	C5–S1	1.371
C5–C6	1.401	C5–C6	1.389
C6–N1	1.394	C6–N1	1.393
Bond angle	**degrees**	**Bond angle**	**degrees**
C1–Al–O1	119.9	C1–Al–O1	119.7
C1–Al–O3	122.9	C1–Al–O2	116.9
C1–Al–N1	93.6	C1–Al–N1	98.5
C1–Al–N2	96.8	C1–Al–N2	95.9
O1–Al–O3	117.2	O1–Al–O2	123.4
O1–Al–N1	88.0	O1–Al–N1	87.3
O1–Al–N2	86.4	O1–Al–N2	85.8
O3–Al–N1	86.9	O2–Al–N1	85.8
O3–Al–N2	87.9	O2–Al–N2	87.2
N1–Al–N2	169.6	N1–Al–N2	165.6
C2–N1–C6	112.5	C2–N1–C6	106.2
C2–O2–C5	89.8	C2–S1–C5	105.9

Table S9 Selected bond lengths and bond angles of the stationary points in the insertion step of the first L-LA mediated by **1a**–**1b'**.

Reaction coordinate	Parameter	Initiator			
		1a	**1a'**	**1b**	**1b'**
R	*Bond length* (Å)				
	Al–O1	1.793	1.808	1.788	1.806
	Al–N1	2.046	2.039	2.059	2.005
	Al–O3	1.771	1.777	1.787	1.787
	Al–O4	2.313	2.224	3.143	3.223
	O3–C	2.665	2.629	2.682	2.702
	O4–C	1.209	1.212	1.198	1.196
	Bond angle (degrees)				
	O1–Al–O4	85.0	85.9	162.0	161.6
	O3–Al–O4	83.1	83.4	67.3	66.8
	N1–Al–O4	173.0	172.5	108.3	108.6
TS1	*Bond length* (Å)				
	Al–O1	1.792	1.800	1.817	1.829
	Al–N1	2.102	2.081	2.061	2.006
	Al–O3	1.871	1.866	1.909	1.903
	Al–O4	1.955	1.959	1.985	2.009
	O3–C	1.859	1.860	1.953	1.941
	O4–C	1.257	1.257	1.250	1.249
	Bond angle (degrees)				
	O1–Al–O4	96.9	94.4	169.2	166.7
	O3–Al–O4	74.0	74.3	73.2	72.7
	N1–Al–O4	160.4	161.6	93.1	92.3
INT1	*Bond length* (Å)				
	Al–O1	1.779	1.786	1.782	1.801
	Al–N1	1.976	1.963	2.057	2.011
	Al–O3	2.801	2.847	2.810	2.851
	Al–O4	1.753	1.751	1.788	1.788
	O3–C	1.430	1.430	1.417	1.415
	O4–C	1.347	1.347	1.350	1.347
	Bond angle (degrees)				
	O1–Al–O4	113.8	112.3	128.5	123.0
	O3–Al–O4	52.6	51.5	52.4	51.4
	N1–Al–O4	108.9	108.6	92.9	94.3

Table S10 Selected bond lengths and bond angles of the stationary points in the ring-opening step of the first L-LA mediated by **1a**–**1b'**.

Reaction coordinate	Parameter	Initiator			
		1a	**1a'**	**1b**	**1b'**
INT2	*Bond length* (Å)				
	Al–O1		1.778	1.775	1.796
	Al–N1		1.958	2.050	2.001
	Al–O4		1.479	1.781	1.786
	Al–O5		2.949	3.005	3.020
	O5–C		1.430	1.427	1.427
	O4–C		1.342	1.338	1.335
	Bond angle (degrees)				
	O1–Al–O4		114.8	119.3	116.8
	O4–Al–O5		50.1	48.2	47.9
	N1–Al–O4		105.7	95.6	96.4
TS2	*Bond length* (Å)				
	Al–O1	1.792	1.797	1.816	1.825
	Al–N1	2.140	2.105	2.065	2.011
	Al–O4	1.947	1.938	2.053	2.096
	Al–O5	1.935	1.937	1.906	1.901
	O4–C	1.267	1.270	1.233	1.230
	O5–C	1.780	1.770	2.152	2.152
	Bond angle (degrees)				
	O1–Al–O4	93.8	92.6	173.6	171.7
	O4–Al–O5	73.4	73.6	77.7	76.9
	N1–Al–O4	157.3	159.8	90.9	91.4
P	*Bond length* (Å)				
	Al–O1	1.792	1.806	1.810	1.819
	Al–N1	2.045	2.019	2.061	2.015
	Al–O4	4.471	4.470	4.357	4.182
	Al–O5	1.789	1.791	1.822	1.827
	O4–C	1.198	1.198	1.199	1.201
	O5–C	4.930	4.910	4.820	4.681
	$Al–O_{carbonyl}$	2.105	2.094	2.081	2.095
	Bond angle (degrees)				
	$O1–Al–O_{carbonyl}$	86.6	86.5	174.6	173.7
	$O5–Al–O_{carbonyl}$	81.5	81.7	80.5	80.4
	$N1–Al–O_{carbonyl}$	167.4	166.4	92.0	90.5

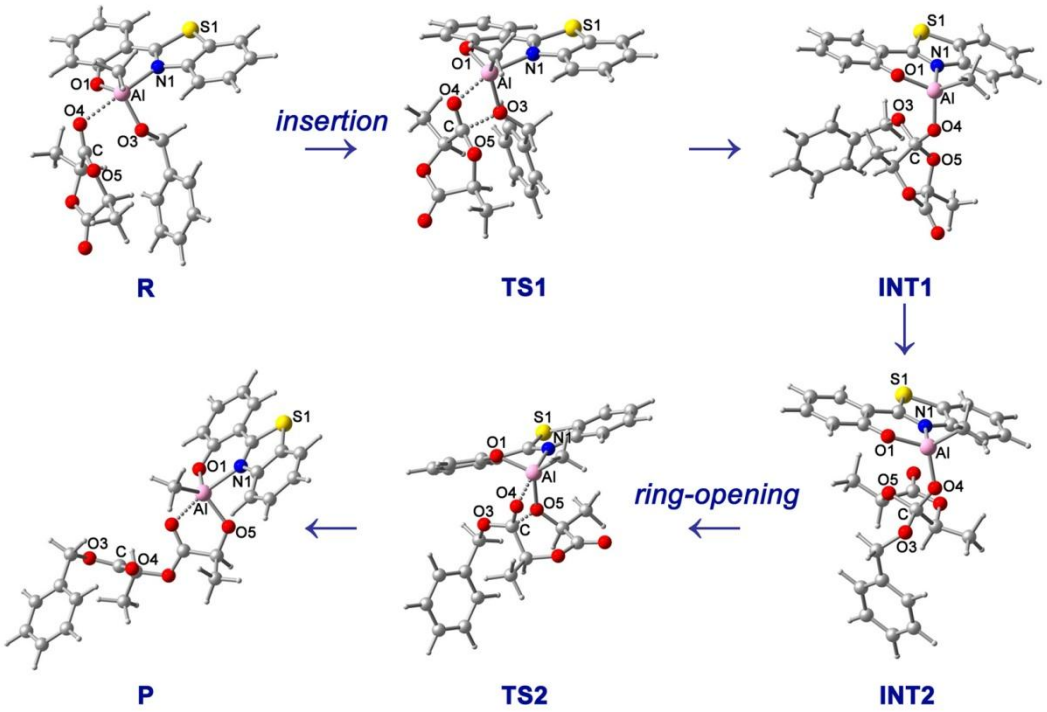

Fig. S57 Schematic illustration of the optimized structures of transition states and intermediates along the ROP of the first L-LA mediated by **1a**.

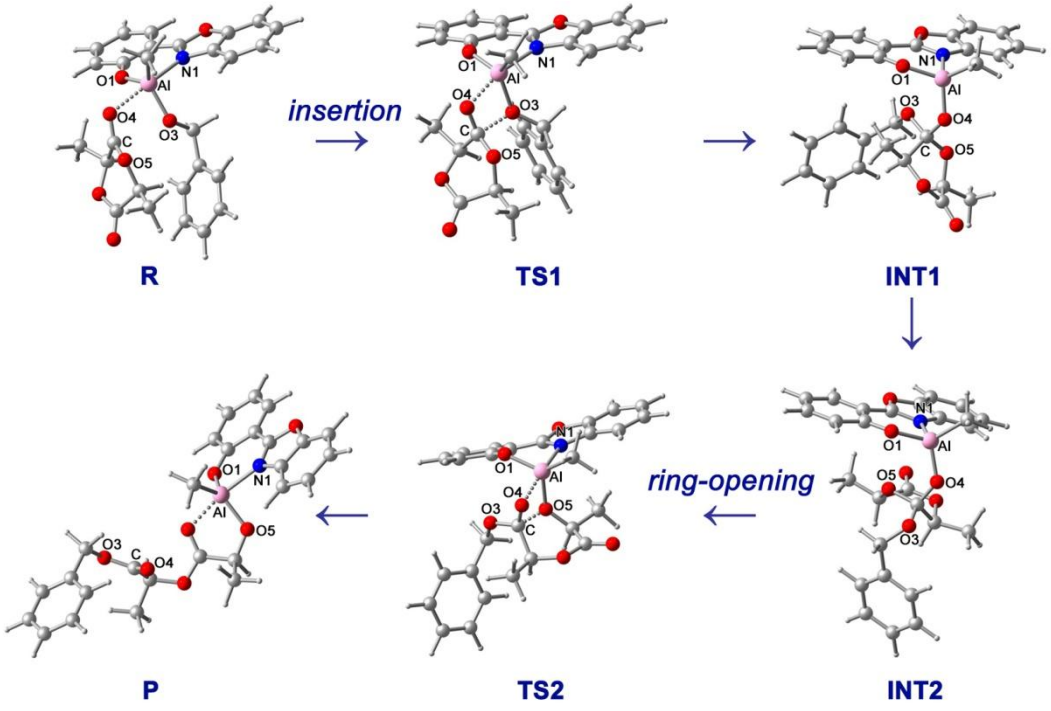

Fig. S58 Schematic illustration of the optimized structures of transition states and intermediates along the ROP of the first L-LA mediated by **1a′**.

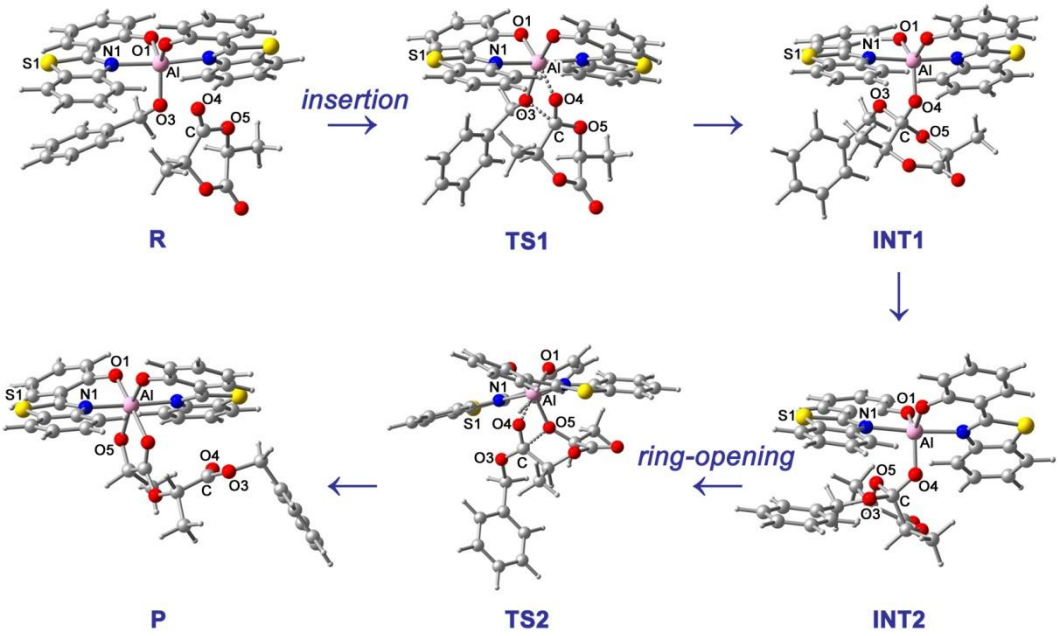

Fig. S59 Schematic illustration of the optimized structures of transition states and intermediates along the ROP of the first L-LA mediated by **1b**.

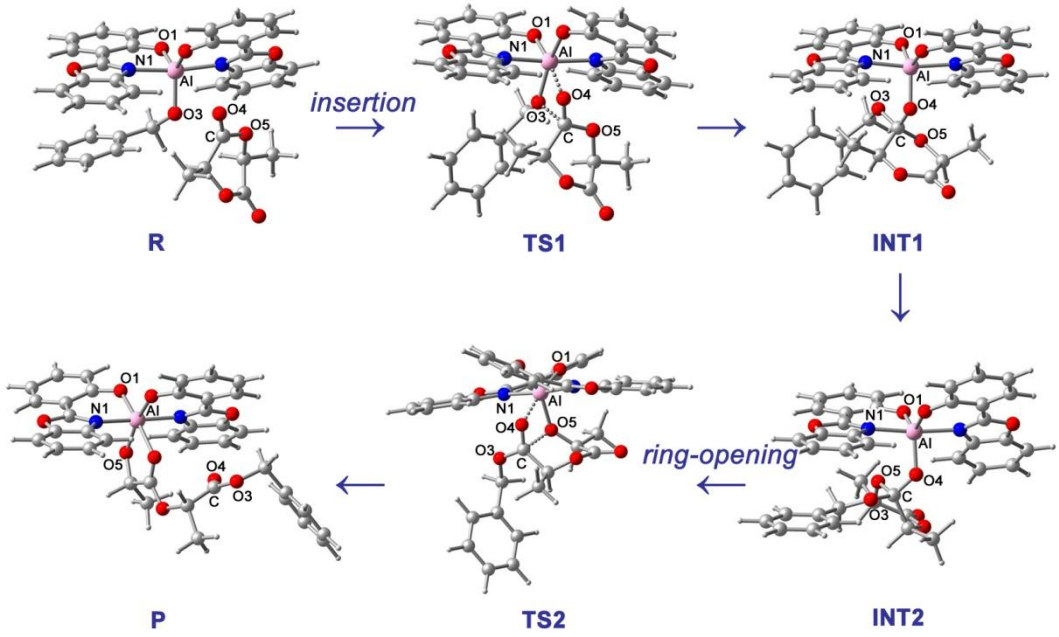

Fig. S60 Schematic illustration of the optimized structures of transition states and intermediates along the ROP of the first L-LA mediated by **1b′**.